Spectral Transitions in Cygnus X#1 and Other Black Hole X#Ray Binaries

Spectral Transitions in Cyg X-1 and Other Black Hole X-Ray Binaries

Ann A. Esin, Ramesh Narayan
Harvard-Smithsonian Center for Astrophysics, 60 Garden St, Cambridge, MA 02138

Wei Cui
Center for Space Research, Massachusetts Institute of Technology, Cambridge, MA 02139

J. Eric Grove
Naval Research Laboratory, Washington, DC 20375-5352

Shuang-Nan Zhang
ES-84, NASA/Marshall Space Flight Center, Huntsville, AL 35812

ABSTRACT

We show that the model proposed by Esin, McClintock & Narayan (1997) for the low state, intermediate state and high state of the black hole soft X-ray transient, Nova Muscae 1991, is consistent with the spectral evolution of the black hole X-ray binary, Cyg X-1, during the hard-to-soft state transition observed in 1996. We also apply the model to the outbursts of two other black hole X-ray transients, GRO J0422+32 and GRO J1719−24.

Subject headings: accretion, accretion disks – black hole physics – X-rays: stars

1. Introduction

Galactic X-ray sources that contain accreting black holes are among the most interesting objects in high energy astrophysics. An X-ray source is classified as a black hole X-ray binary (BHXB) if the observed mass function, or other less direct dynamical evidence, places the mass of the compact object above $3M_{\odot}$ (examples are A0620−00, 4U 1543−47, V404 Cyg, Nova Muscae 1991, GRO J1655−40, GS 2000+251, Cyg X-1, GRO J0422+32, H1705−250 and LMC X-3), or if the spectral and temporal characteristics of the source are similar to those of the well established BHXBs (e.g. GX 339−4, 1E 1740.7−2942, GRS 1915+105, GRO J1719−24). Recent reviews of this subject are given by Tanaka & Lewin (1995), Tanaka & Shibazaki (1996), and Liang (1997).

BHXBs are known to exhibit five distinct X-ray spectral states, distinguished by the presence or absence of a soft blackbody component at ~ 1 keV and the luminosity and spectral slope of emission at harder energies. Systems in the *low/hard state* have hard power-law spectra with a photon index $\Gamma \sim 1.4 - 1.9$, an exponential cutoff around 100 keV, and no (or only weak) evidence of a soft thermal component. On the other hand, *high/soft state* spectra are dominated by a blackbody component with a characteristic temperature ~ 1 keV (Tanaka & Shibazaki 1996). At higher energies, high state spectra show a power-law tail, softer than in the low state ($\Gamma \sim 2.2 - 2.7$), but often extending above 500 keV without an obvious turnover. Of these two spectral states, the high state is generally more luminous, with $L_X \sim 0.2 - 0.3 L_{\rm Edd}$, while systems in the low state have X-ray luminosities below $\sim 0.1 L_{\rm Edd}$ (e.g. Nowak 1995); this trend is of course based on systems for which distance and black hole mass estimates are available. Recently, *intermediate state* spectra have been seen in several systems (e.g. Nova Muscae, Ebisawa et al. 1994; GX 399−4, Mendez & van der Klis 1997; Cyg X-1, Belloni et al. 1996), which, as the name suggests, are intermediate both in spectral shape and luminosity between the high and low state spectra.

Two other spectral states have been seen in some BHXBs. At least two sources, Nova Muscae and GX 339−4 (Ebisawa et al. 1994; Miyamoto et al 1991), have been observed in the *very high state*, with luminosities close to the Eddington limit. This state has similar spectral properties as the high state, but is characterized by higher bolometric luminosity and more prominent hard tail, stronger variability and the presence of $3 - 10$ Hz QPOs (e.g. van der Klis 1994; Gilfanov et al. 1993). In addition, all transient BHXBs (e.g. Nova Muscae, A0620−00, V404 Cyg) spend most of their time in a *quiescent/off state*, characterized by a very low X-ray flux (e.g. McClintock, Horne & Remillard 1995; Narayan, Barret & McClintock 1997a; Narayan, Garcia & McClintock 1997b).

In the past several decades X-ray and γ-ray observations have considerably improved our understanding of BHXBs, and significant progress has been made in theoretical modeling of different spectral states. It has been generally accepted that the soft thermal component originates in an optically thick, geometrically thin accretion disk (Shakura & Sunyaev 1973; Novikov & Thorne 1973), while the power-law high energy emission is produced by Comptonization of soft photons in a hot corona (e.g. Shapiro, Lightman, & Eardley 1976; Haardt et al. 1993; Melia & Misra 1993). However, the spatial relationship between the hot and cold medium in the accretion flow has until recently been unclear.

Narayan, McClintock & Yi (1996) and Narayan et al.(1997a) showed that to produce the observed optical and X-ray emission in quiescent soft X-ray transients (SXTs), the accreting gas must be primarily in the form of an optically thin hot flow which extends

out to a large radius, of order several thousand Schwarzschild radii; beyond this radius, the accretion occurs via a thin disk. These authors modeled the hot accreting gas as an optically thin advection-dominated accretion flow (ADAF). This is an accretion solution which was discovered by Ichimaru (1977) and Rees et al. (1982), and then rediscovered and further studied by Narayan & Yi (1994, 1995a, 1995b), Abramowicz et al. (1995), Chen (1995), Chen et al. (1995) and others. Hot optically thin ADAFs exist only below a certain critical accretion rate, $\dot{m}_{\rm crit} \sim 0.1$ in Eddington scaled-units. Because the density of the gas is low, the flow is unable to cool efficiently. Instead, most of the viscously dissipated energy is stored in the gas as thermal energy of the gas particles and is advected into the black hole through the event horizon. As a result, the radiative efficiency of an ADAF around a black hole is significantly lower than that of a standard thin disk. This makes the ADAF model especially appropriate for modeling under-luminous quiescent systems.

The model proposed by Narayan et al. (1996, 1997a) for quiescent SXTs was used by Hameury et al. (1997) to explain the light curve of the transient source, GRO J1655-45, during its recent outburst. Previously, Mineshige & Wheeler (1989) and Huang & Wheeler (1989) had suggested that outbursts in transients are due to a thermal instability in the thin accretion disk and extended a model developed previously for dwarf novae to black hole transients. However, if the thin disk extends down to the last stable orbit in quiescence, the predicted recurrence time between outbursts is inconsistent with observations (Lasota, Narayan, & Yi 1996; Mineshige 1996). The predicted and observed time scales are in better agreement if the thin disk is truncated at a large transition radius, $R_{\rm tr}$.

In ADAF models of quiescent SXTs, the mass accretion rate is fairly low, $\dot{m} \lesssim 10^{-3}$ in Eddington units (Narayan et al. 1996, 1997a). Narayan (1996) proposed that at higher accretion rates the same model might naturally explain the more luminous spectral states of black hole binaries. This suggestion was worked out in detail by Esin, McClintock & Narayan (1997, hereafter EMN). They showed that the low state is similar to the quiescent state in its flow configuration, but with a mass accretion rate roughly two orders of magnitude higher, namely $0.05 \lesssim \dot{m} \lesssim 0.1$, where $\dot{m}$ is in Eddington units. Similar models were proposed for the low state of Cyg X-1 by Shapiro et al. (1976) and Ichimaru (1977). In particular, Ichimaru (1977) was the first to recognize the importance of advection dominated accretion for understanding BHXBs; sadly, his paper was forgotten for many years. At yet higher accretion rates, an ADAF cannot be maintained at large radii; the transition radius (i.e. the inner edge of the thin disk) then comes closer to the black hole. The spectra produced by such models resemble well the intermediate state spectra observed in some systems. Finally, for yet higher mass accretion rates, the thin disk extends all the way down to the last stable orbit and the ADAF is restricted to a corona above the disk. Such a configuration describes the high state.

EMN demonstrated that their model, consisting of an inner ADAF surrounded by an outer thin disk, can reproduce the low, intermediate and high state spectra of BHXBs. Moreover, they showed that the existence of the critical accretion rate $\dot{m}_{\rm crit}$ above which the ADAF solution disappears provides a natural explanation for spectral transitions between the high and low state. EMN modeled the outburst of Nova Muscae 1991 using this scenario and showed that the model successfully reproduces the observations of the system in the three spectral states.

Recent observations of several BHXBs have confirmed the basic conclusions of EMN. By studying the fluorescent Fe Kα line and Compton reflection component in the low state spectrum of Cyg X-1, Gierliński et al. (1997a) concluded that the cold reflecting medium does not extend down to the marginally stable orbit (for a non-rotating black hole) in the low state. The same conclusion was also reached by Dove et al. (1997a, 1997b), who found that the reprocessing of the hot radiation in the cold medium is too weak, and, therefore, that the cold disk must be truncated relatively far outside $3R_{\rm Schw}$. A more direct confirmation came from Zhang et al. (1997a, 1997b) and Życki et al. (1997) who studied the transition between the low and high spectral states in Cyg X-1 and Nova Muscae respectively, and found a larger value for the transition radius in the low state than in the high state. This confirms the overall qualitative features of the EMN model.

We begin this paper in §2 with a review of the predictions of the EMN model; in particular, we discuss the spectral signatures predicted for various state transition, and show how they can be used as diagnostics when the available spectral information is incomplete. In §3 we concentrate on the recent hard–soft spectral state transition in Cyg X-1. We show that the data are consistent with the basic scenario described above, namely that during the transition Cyg X-1 went from the low state, with a relatively large inner radius for the thin disk and an accretion rate near the critical value, to a series of intermediate states with smaller transition radii, and culminated in the high state with $R_{\rm tr} = 3R_{\rm Schw}$. We show that this model convincingly explains the overall spectral evolution of the system, as well as reproduces its hard and soft state spectra fairly well.

In §4 we discuss the application of the model to another black hole system, GRO J0422+32, during its 1992 outburst. We demonstrate that the spectrum of GRO J0422+32 near the peak of the outburst is well modeled by a low state spectrum with $\dot{m} \sim \dot{m}_{\rm crit}$. We then argue that since the spectrum remained a hard power-law throughout the outburst, the accretion rate never increased significantly above its critical value. Thus GRO J0422+32 never went into an intermediate or high spectral state. We show that this conclusion is consistent with the observed anti-correlation between the cutoff energy and the X-ray luminosity during the decay after the outburst.

Finally, in §5 we show that the EMN model also provides some clues to the secondary outbursts observed in GRO J1719−24 (also known as GRS 1716-249 or Nova Ophiuchi 1993). Though the spectral evolution of the system since its discovery in September 1993 is not well-documented in the literature, we show that the known facts are consistent with an outburst from the quiescent to the very high spectral state, like those seen in "typical" SXTs (e.g. Nova Muscae or A0620−00), followed by a series of low-high state transitions, similar to those observed in Cyg X-1. We conclude in §6 with a summary.

2. Spectral States and State Transitions of BHXBs

We begin with a brief description of the model geometry and the calculations (see EMN for details).

2.1. ADAF Model Overview

2.1.1. Flow Geometry

We consider a Schwarzschild black hole of mass $M = mM_\odot$ accreting matter from its binary companion at a rate $\dot{M} = \dot{m}\dot{M}_{Edd}$, where $\dot{M}_{Edd} = L_{Edd}/(0.1c^2) = 1.39 \times 10^{18} m$ is the Eddington accretion rate computed for 10% radiative efficiency. The binary orbital angular momentum vector is inclined at an angle i to the observer's line of sight.

The basic picture of mass accretion via an ADAF in the context of BHXBs was worked out in a series of papers by Narayan and collaborators (Narayan et al. 1996; Narayan 1996; Narayan et al. 1997a; Hameury et al. 1997; EMN). In this scenario, the accretion flow is divided into two distinct zones. The inner part is modeled as a hot optically thin ADAF extending down to the black hole horizon, while the outer part consists of an optically thick, geometrically thin disk with a hot corona (modeled as an ADAF) above it. The transition radius between the two zones, $r_{\rm tr} = R_{\rm tr}/R_{\rm Schw}$ (hereafter all radii are in Schwarzschild units), is one of the model parameters. Another less important parameter is the radius of the outer edge of the accretion flow, $r_{\rm out}$.

Though the total mass accretion rate in the disk and corona is constant at each radius (this is not strictly true in time-dependent flows, but we make this assumption for simplicity), it is not possible to determine from first principles the fraction of mass accreted through the corona. This is because the coupling between the hot corona and the cold disk through evaporation and thermal conduction (see e.g. Meyer & Meyer-Hofmeister 1994),

is poorly understood. We simply assume that the coronal mass accretion rate is inversely proportional to the radius, i.e.

$$\dot{m}_c(r) = \dot{m}\left(\frac{r_{\rm tr}}{r}\right), \qquad r > r_{\rm tr}. \tag{2-1}$$

(The results are not very different if we assume other radial profiles for $\dot{m}_c$.)

2.1.2. Flow Dynamics and Energy Balance

Once the total accretion rate $\dot{m}$ and accretion rate in the corona $\dot{m}_c(r)$ are set, all the relevant properties of the hot flow can be computed. The ADAF is treated as a collection of spherical shells, truncated near the pole to mimic the flattening of the density profile. Each shell is characterized by its radial and azimuthal velocity, gas density, electron and proton temperatures, magnetic field strength, etc. These quantities are determined by solving the global dynamical conservation laws of mass, angular momentum, radial momentum and energy, together with the radiative transfer problem. The manner in which the solutions are obtained is described in detail in Narayan, Kato & Honma 1997c, Narayan et al. (1997a) and EMN; here we present a brief summary and introduce the model parameters.

In each shell the viscous energy dissipation is computed using the standard α-prescription. We assume that most of the energy is deposited in the protons (see Bisnovatyi-Kogan & Lovelace 1997, Quataert 1997, Gruzinov 1997 and Blackman 1997 for recent discussions of this assumption); the protons then reach nearly virial temperature through viscous heating and adiabatic compression. We further assume that the electrons and protons are coupled only through Coulomb collisions, which is inefficient in a hot, low-density plasma. Thus, only a fraction $(1 - f)$ of the viscous energy is transferred to the electrons, and the rest is carried inside the black hole horizon as entropy of the gas. The quantity f is called the advection parameter, and is solved for self-consistently.

The electrons in the flow cool via three processes: bremsstrahlung, synchrotron radiation, and inverse Compton scattering. To compute the synchrotron emissivity of the gas (Mahadevan, Narayan & Yi 1996), we assume that the tangled magnetic field is roughly in equipartition with the hot gas, so that the ratio of the gas to total pressure, β, is of order 0.5. In calculating the rate of cooling due to Compton scattering we take into account the coupling between different shells of the ADAF, as well as the interaction between the hot flow and the thin disk (Narayan et al. 1997a, EMN).

The radial profiles of electron and proton temperature in the ADAF are determined by demanding that the energy equations for both protons and electrons are satisfied in each

radial shell. The rate of change of entropy of the protons is set equal to the viscous energy dissipation minus losses through Coulomb collisions with electrons. For the electrons, the entropy change is set equal to the energy gain through Coulomb coupling with the protons, plus the fraction δ of the viscous energy dissipation that goes directly into heating the electrons, minus radiative cooling. In our calculations we adopt $\delta = 10^{-3}$, though the results are not sensitive to the exact value of this parameter as long as $\delta \lesssim 10^{-2}$.

2.1.3. Emission from the Thin Disk

The emission from the thin disk is calculated using the standard multicolor blackbody method (e.g. Frank et al. 1992) corrected for graybody effects due to electron scattering (e.g. Shimura & Takahara 1995); in addition, we include the Compton reflection component due to the scattering of hot ADAF photons incident on the disk surface, and fluorescent iron Kα line emission. In EMN the thin disk was treated as an infinitely thin plane. Here we take into account the finite disk thickness, which we assume to be equal to the local pressure scale height. The scale height itself is calculated self-consistently including the effect of irradiation of the disk by radiation from the ADAF.

The modified blackbody spectrum of the disk is computed using the standard expression:

$$L_{\nu,\mathrm{disk}}(r)dr = \left(\frac{1}{f_{\mathrm{mbb}}}\right)^4 B_\nu(f_{\mathrm{mbb}}\ T_{\mathrm{eff}}(r)) \cdot 2\pi \cdot 2\pi r dr, \tag{2-2}$$

where B_ν is the Planck function, $T_{\mathrm{eff}}(r)$ is the effective surface temperature of the disk at radius r (which includes both the local viscous dissipation as well as the fraction of the irradiating flux which is absorbed), and f_{mbb} is a factor which allows for modified blackbody effects; we set f_{mbb} equal to 1.7 following Shimura & Takahara (1995).

Not all photons incident on the thin disk are absorbed and reprocessed. A significant fraction of the incident energy is Compton scattered in the upper disk layers and is effectively reflected back with lower energy than that of the incident photons. The result is a broad peak centered at around 30 keV. We compute this part of the spectrum by convolving the incident spectrum with the angle-averaged Greens function for Compton reflection of monoenergetic photons from a cold, neutral, optically thick medium (White, Lightman & Zdziarski 1988; Lightman & White 1988). The metal abundances are taken from Morrison & McCammon (1983).

Finally, we compute the strength and shape of the fluorescent iron line produced through photoelectric absorption of the incident X-ray photons with energies above

the K-shell absorption edge, $E_K = 7.1$ keV. We compute the line strength using the empirical formula given by George & Fabian (1991), and the line profile taking into account gravitational redshift and Doppler shifts due to rotation (Fabian et al. 1989). However, we ignore the effects of ray bending in the vicinity of the black hole; this effect becomes important only when the transition is below $r = 10$ (Fabian et al. 1989).

2.2. Spectral States of BHXBs

EMN calculated the spectra of the above model as a function of the two main parameters, $\dot{m}$ and $r_{\rm tr}$, and identified different regions of parameter space with the known spectral states of black hole systems. Here we summarize their scenario for the quiescent, low, intermediate and high spectral states. We ignore the very high state, which is not relevant for this paper (this state was in any case, not explained very convincingly by EMN).

At low mass accretion rates ($\dot{m} \lesssim 10^{-2}$) and relatively large transition radii ($r_{\rm tr} \gtrsim 10^3$) the model spectra strongly resemble the quiescent states of transient black hole systems (e.g. A0620-00, V404 Cyg, GRO J1655-40; see Narayan et al. 1996, Narayan et al. 1997a; Hameury et al. 1997). In this region of parameter space, the optical/UV part of the spectrum is dominated by self-absorbed synchrotron emission from the ADAF (NBM) and the X-rays are produced by bremsstrahlung emission and Comptonized synchrotron photons. The contribution from the thin disk is negligible. The spectral slope in the X-ray band varies strongly with the accretion rate (see Figure 1a). For $\dot{m} \lesssim 10^{-3}$, bremsstrahlung dominates and the spectral slope is roughly constant with photon index $\Gamma \sim 1.7$ (N.B. in EMN the photon index was denoted by the symbol α_N). In the range $10^{-3} \lesssim \dot{m} \lesssim 10^{-2}$, the X-ray spectrum is dominated by Compton scattered synchrotron photons, and the photon index increases to $\Gamma \sim 2.2$, producing a steeper spectrum. The radiative efficiency of the ADAF is proportional to $\dot{m}$ (Narayan & Yi 1995b), so that the quiescent state spectra have very low luminosities, $L \sim L_{\rm Edd}(\dot{m}^2/0.1)$, consistent with what is observed.

Models with $\dot{m} \gtrsim 10^{-2}$ and $r_{\rm tr} > 100$ are associated with the low state of BHXBs. In this regime, the X-ray part of the spectrum is formed by Comptonized synchrotron photons. Therefore, with increasing $\dot{m}$ as the optical depth and Compton y-parameter increase the spectral slope flattens (Figure 1a). The emission is dominated by high energy photons at ~ 100 keV. The thin disk may contribute significantly to the observed emission in the optical/UV band, though the exact contribution depends on the value of $r_{\rm tr}$ (compare Figures 1a and 1b). However, the shape of the X-ray spectrum is not sensitive to the location of the transition radius, as long as $r_{\rm tr} \gtrsim 100$. In fact, even with $r_{\rm tr} \sim 30$, the slope

in the 1-10 keV range remains hard, and the only noticeable difference is in the appearance of an ultrasoft disk component below 1 keV, the presence of a reflection bump at ~ 30 keV and the strength of iron fluorescent line.

It has been demonstrated in several papers that two-temperature ADAFs exist only for accretion rates below some critical value $\dot{m}_{\rm crit}$ (Ichimaru 1977, Rees et al. 1982, Narayan & Yi 1995b, Chen et al. 1995, EMN). Above $\dot{m}_{\rm crit}$ the accreting gas cools so rapidly, that the flow cools down to form the standard optically-thick Shakura-Sunyaev disk. EMN demonstrated that $\dot{m}_{\rm crit}$ is a function of the transition radius between the hot and cold flow, increasing slightly with decreasing $r_{\rm tr}$. Thus, they proposed that when the accretion rate in BHXBs increases above the critical value for a given value of $r_{\rm tr}$, the outer parts of the hot flow start cooling down to form a thin disk, i.e. $r_{\rm tr}$ decreases in an attempt to keep $\dot{m}$ at $\dot{m}_{\rm crit}$. When $r_{\rm tr}$ falls below about 30, the model spectra resemble the intermediate state spectra observed in several black hole systems, e.g. Nova Muscae (Ebisawa et al. 1994), Cyg X-1 (Belloni et al. 1996), GX 339−4 (Mendez & van der Klis 1997).

Since $\dot{m}_{\rm crit}$ changes by at most $\sim 15\%$ while $r_{\rm tr}$ decreases by a large factor the bolometric luminosity is roughly the same for all intermediate state spectra. The spectral shape, however, is strongly dependent on the value of $r_{\rm tr}$. For $r_{\rm tr} > 30$ the X-ray spectra are similar to those in the low state (large $r_{\rm tr}$), with $\Gamma \sim 1.5$, while by the time $r_{\rm tr} \sim 3$, the spectrum is dominated by the soft blackbody component from the disk at ~ 1 keV, with a steep power-law tail characterized by $\Gamma \sim 2.3$.

When the thin disk extends down to the last stable orbit, the ADAF is restricted to the corona above the disk. EMN associate this flow configuration with the high state, in which blackbody radiation from the disk dominates the spectrum and the corona produces only a weak high energy tail. Because the electron temperature in the ADAF is rather low in the high state configuration, the power-law tail in our model spectra turns over at ~ 100 keV, while the observed spectra extend to ~ 500 keV without a cut-off (e.g. Grove et al. 1997). This discrepancy either indicates the presence of non-thermal electrons, or more likely is due to bulk motion Comptonization of the thin disk photons, as suggested by Ebisawa, Titarchuk & Chakrabarti (1996). The radial velocity of the ADAF gas is on the order of the free fall velocity, and since the electron temperature in the high state decreases, the bulk motion Comptonization (which we do not take into account in our model) might become more important than thermal Comptonization.

In their model for the spectral evolution of Nova Muscae during its 1991 outburst, EMN assumed that the plateau in the lightcurve of the system observed between days 130 and 200, corresponds to the transition from the high to the low spectral state, with $r_{\rm tr}$ increasing from 3 to $\sim 10^4$ (the upper value was determined from the quiescent state

spectrum, see Narayan et al. 1996). This assumption was made for the sake of simplicity, since the data used in the paper were not good enough to place better constraints on $r_{\rm tr}$ in the low state. Recent detailed analysis by Życki et al. (1997), seems to imply that by day 200, $r_{\rm tr}$ increased only up to ~ 20. To reconcile this result with the value of $r_{\rm tr}$ in quiescence, we must conclude that the thin disk continued to evaporate after day 200, while the mass accretion rate dropped from its value in the low state, to that in quiescence. As pointed out above, as long as $r_{\rm tr} \gtrsim 30$ in the low state, the exact position of the transition radius does not significantly change the X-ray spectrum (compare Figures 1a and 1b). Thus this slight modification of the model has no effect on the main results of EMN.

In the discussion above we have outlined how the spectrum of the ADAF plus the disk changes as a function of $\dot{m}$ and $r_{\rm tr}$. The other parameters, such as m, $r_{\rm out}$, i, α and β, do not significantly affect the main features of the model spectra. For example, changing the mass of the accreting black hole affects only the normalization of the spectrum and the effective temperature of the thin disk ($T_{\rm eff} \propto m^{-1/4}$, Frank et al. 1992). Larger values of α and β produce slightly harder low state spectra, and raise the value of $\dot{m}_{\rm crit}$ (see Narayan 1996; Narayan et al. 1997a and EMN for detailed discussion), but the overall behavior of the model is unaffected.

In the calculations presented below, we generally set $\beta = 0.5$ and $\alpha = 0.3$, which we consider to be the most natural values for these parameters. The former simply restates our assumption of equipartition between magnetic and gas pressure, a common assumption in many areas of high-energy astrophysics. For the viscosity parameter α we follow the prescription suggested by Hawley & Balbus (1996), $\alpha \sim c(1-\beta)$ with c between 0.5 and 0.6. For the other two parameters, m and i, we adopt values suggested by observations of the systems we model.

2.3. Spectral Signatures During State Transitions

Though some black hole candidates are always observed in the same spectral state (e.g. LMC X-3 and 1E 1740.7−2942), the majority of observed BHXBs exhibit some degree of long-term spectral variability. The most dramatic behavior is observed in soft X-ray transients (also known as "X-ray novae"), which in some cases have been detected in all five spectral states, including the "very high state" not discussed in this paper. A typical example of such a system is Nova Muscae (e.g. Ebisawa et al. 1994, EMN). Most other black hole systems exhibit two or three spectral states. For example, Cyg X-1 routinely switches between the low state and high state, passing through a series of intermediate states (e.g. Phlips et al. 1996; Zhang et al. 1997a, see also review by Tanaka & Lewin

1995 and references therein); the high and low states were also detected during OSSE observations of GRO J1719−24 (Grove et al. 1997). On the other hand, the transient source GRO J0422+32 has been seen only in the quiescent state and low state (Grove et al. 1997; Tanaka & Shibazaki 1996 and references therein). However, regardless of the number of distinct states observed, we believe most systems are described by the model outlined in §2.2.

Figures 1a and 1b illustrate the model predictions for the various spectral states. Shown are a sequence of spectra computed for $m = 9$, $i = 40^\circ$ and values of $r_{\rm tr}$ and $\dot{m}$ as stated in the figure caption. Starting with the lowest spectrum, which corresponds to the quiescent state, one can follow the spectral evolution all the way to the luminous high state. Apart from the monotonic increase in the overall luminosity, the most striking changes are seen in the spectral slope in the X-ray band. The spectrum is hard in the quiescent state, becomes softer as the mass accretion rate increases (the photon index reaches its maximum $\Gamma \sim 2.2$ for $\dot{m} \sim 10^{-2}$), and switches again to a very hard spectrum in the low state. During the transition from the low to the high state, the spectrum softens again and continues to soften with increasing $\dot{m}$ in the high state. Note that the exact value of $r_{\rm tr}$ in the low and quiescent states changes only the characteristic frequency of the thin disk component (generally located in the UV or optical part of the spectrum) and not the shape of the X-ray emission.

A less obvious, but nonetheless important change takes place in the position of the high energy thermal cut-off in the spectrum. In the quiescent state, the cooling of the flow is very inefficient and the electron temperature in the inner regions of the ADAF is relatively high, reaching $4 - 6 \times 10^9$ K. However, with increasing $\dot{m}$ the electron temperature drops due to increased cooling, and the exponential cut-off occurs at lower energies. The resulting relationship between the average electron temperature of the flow inside $10R_{\rm Schw}$, and the X-ray luminosity at 100 keV (the band which is most sensitive to changes in $\dot{m}$), is shown in Figure 2. Clearly, during the transition from the quiescent to the low state, T_e and the hard X-ray luminosity are *anti-correlated*.

During the transition through the intermediate states, when $r_{\rm tr}$ decreases without significant change in $\dot{m}$, T_e continues to fall. As the blackbody disk component becomes more prominent, the hot accretion flow is cooled progressively more efficiently by the soft photons from the thin disk. Both the hard X-ray flux and the temperature decrease. Therefore, in the intermediate spectral state, the flux at 100 keV and T_e are *correlated* with each other, as clearly shown in Figure 2.

Though the spectra corresponding to different states are very distinct when compared over a wide range of frequencies, say from optical to X-rays, in real life one generally has

much more limited information, e.g. just the hard X-ray flux. When the data are restricted to a relatively narrow energy band, different spectral transitions may look rather similar. The relationship between T_e and the hard X-ray flux illustrated in Figure 2 could then be used as a diagnostic to determine the nature of the transition.

3. Application to Cyg X-1 1996 State Transition

Cyg X-1, discovered by Bowyer et al. (1965), is one of the oldest known X-ray sources and perhaps the most thoroughly studied Galactic black hole candidate. The system consists of a compact object orbiting around an O9.7 Iab supergiant (Walborn 1973; Gies & Bolton 1986a) with a period of 5.6 days. The X-ray emission is most likely powered by focused wind accretion from the optical companion (Gies & Bolton 1986b). The extinction towards Cyg X-1 places this system at a distance of $\gtrsim 2.5$ kpc (Margon & Bowyer 1973; Bregman et al. 1973); we use 2.5 kpc for comparisons between the model and observations.

From the orbital motion of the primary, the mass function of the compact object is measured to be $f(M) = 0.25 \pm 0.01 M_\odot$ (Gies & Bolton 1982), and recent estimates (e.g. Herrero et al. 1995) place the mass of the optical companion at $18 M_\odot$. Unfortunately, the orbital inclination of the system is not well known; the values quoted in the literature vary between 25° and 67° (e.g. Dolan 1992; Ninkov et al. 1987 and references therein). This uncertainty implies that the mass of the black hole candidate can be anywhere in the range between $15 M_\odot$ and $5.5 M_\odot$. For our calculation we adopt $m = 9$ and $i = 40°$.

3.1. Low/Hard Spectral State

Cyg X-1 spends most of its time in the hard state, which is characterized by a hard power-law X-ray spectrum with a photon index $\Gamma \sim 1.4$. The power-law is modified by an exponential cutoff with e-folding energy $E_f \sim 150$ keV (e.g. Phlips et al. 1996; Dove et al. 1997b; Gierliński et al. 1997a, and references therein), and perhaps some soft blackbody emission with characteristic temperature $\sim 0.1 - 0.2$ keV (e.g. Balucinska-Church et al. 1995; Ebisawa et al. 1996). In some hard state spectra of Cyg X-1 there is also a strong indication of spectral hardening above 10 keV, usually interpreted as a Compton-reflection component from a cold disk (Done et al. 1992; Gierliński et al. 1997a). Another evidence for the presence of the disk is the detection of an Fe K-edge at $\gtrsim 7$ keV as well as a narrow Fe Kα fluorescence line (e.g. Barr, White & Page 1985; Ebisawa et al. 1996; Gierliński et al. 1997a).

Historically, the combination of hard power-law continuum and reflection features has been interpreted in terms of a cold disk with a slab-like hot corona model (e.g. Haardt et al. 1993 and references therein; though see also Shapiro et al. 1976 and Ichimaru 1977), where the hard X-ray emission is produced by inverse Compton scattering of the disk photons in the corona, and the irradiation of the thin disk by the hot photons from the corona generates the reflection component and the iron line. However, recent observations and theoretical work have shown that this geometry is not appropriate for explaining the hard state spectra of Cyg X-1. For example, the covering factor inferred by Gierliński et al. (1997a) is too small to be consistent with the slab corona geometry. Similarly, the observed Fe Kα line is too narrow to allow the disk to extend close to the black hole (Ebisawa et al. 1996). More detailed theoretical modeling of the standard disk-corona configuration show that models in which the disk extends all the way to the last stable orbit do not allow a high enough electron temperature in the corona to reproduce the observed hard power-law slope and high energy cut-off (Dove et al. 1997a, 1997b; Poutanen, Krolik & Ryde 1997). The logical conclusion is that the thin disk is truncated at a radius equal to at least a few tens of R_{schw}, and that the inner region of the accretion flow is filled with hot gas.

Qualitatively, this conclusion is in perfect agreement with the prediction of the EMN model for the low spectral state of accreting black hole systems (see §2.3). Figure 3 shows that there is also a reasonable quantitative agreement between the model and the hard state spectra of Cyg X-1. The data shown on the figure correspond to nearly simultaneous Ginga and OSSE observations made on July 6 1991 (Gierliński et al. 1997a). For the spectral fitting we used a grid of ADAF model spectra, characterized by three parameters: $r_{\rm tr}$, the HI column density along the line of sight to Cyg X-1, $N_{\rm H}$ (since the data does not extend below 3 keV, we did not obtain any meaningful constraint on $N_{\rm H}$), and the overall normalization. In each model we fixed $m = 9$, $i = 40^\circ$, $\beta = 0.5$, $\alpha = 0.3$ and set the mass accretion rate to its critical value.

The best fitting model spectrum corresponds to $r_{\rm tr} \sim 100$ and is shown in Figure 3 as a solid line. Clearly, this model does a reasonable job of reproducing both the spectral slope and the shape of the exponential cut-off. The value of the transition radius derived from this fit is consistent with the observed narrow width of the iron fluorescence line (e.g. Ebisawa et al. 1996). To illustrate how sensitive the spectrum is to the value of $r_{\rm tr}$, we show the spectrum corresponding to $r_{\rm tr} = 30$, keeping the other parameters the same (dashed line). This curve produces a slightly worse fit in the high energy end of the spectrum, but the difference between the two model spectra above 2 keV is no greater than 10%, comparable to the uncertainty introduced by the approximations made in our current calculations. For example, using the relativistic global flow solutions in the Kerr geometry (e.g. Gammie & Popham 1997) instead of those based on Newtonian physics, will produce

higher electron temperatures in the ADAF (as demonstrated by Narayan et al. 1997d), and therefore may well change the shape of the high energy cut-off. We would therefore say that Cyg X-1 in the low state must have a transition radius $r_{\rm tr} \gtrsim 20$.

The exact value of the black hole mass does not affect the overall shape of the X-ray spectrum above ~ 2 keV, but the inclination of the system does have a significant effect both on the shape and normalization of the spectrum (e.g. see EMN). Since the density profile in an ADAF is slightly flattened (Narayan & Yi 1995a), for lower values of i the observer sees deeper into the flow, i.e. the observed photons are produced in a hotter medium. Moreover, because of lower optical depth near the pole, the scattered photons escape preferentially in that direction. As a result, systems observed at lower inclination are significantly brighter, and have higher exponential cut-off energies. We find that our fit above 100 keV becomes significantly worse for $i \gtrsim 40^\circ$, which forces us to adopt $m \gtrsim 9$, to be consistent with the other known binary parameters. However, with $m = 9$ and $i = 40^\circ$ the model spectrum shown on Figure 3 is ~ 3 times more luminous than the data. This normalization error is most likely the result of the simplified way we have modeled the flattening of the accretion flow (see §2.1.2 and Narayan et al. 1997a, EMN). Because we have truncated our model near the poles, the effect of changing the inclination in the vicinity of 40° is very dramatic, but perhaps not very realistic. In view of this limitation in the model, as well as possible uncertainty in the distance to Cyg X-1, we feel that the error in the normalization does not represent a serious problem.

Our simplified treatment of the ADAF density profile is also one of the causes for the slight discrepancy between our model spectra and the data in the region around 10 keV. Figure 3 shows that the iron Kα line equivalent width and the depth of the corresponding Fe edge predicted by the model fall short of what is observed, implying that the covering factor of the cold disk is too small. By allowing the photons scattered in the ADAF to escape preferentially in the direction away from the thin disk, the truncation of the hot flow near the poles is at least partially responsible for this discrepancy. Another effect we have not included is partial ionization of the gas in the thin disk. Since highly ionized iron ions have significantly larger fluorescent yields than neutral atoms, taking into account the ionization state of the thin disk may significantly increase the predicted strength of the Fe line (e.g. Życki & Czerny 1994).

3.2. Hard–Soft and Soft–Hard Spectral Transitions

Occasionally, Cyg X-1 undergoes a transition from the hard to the soft spectral state, and the spectrum switches to one which is dominated by an ultrasoft component with a

temperature $\sim 0.3 - 0.4$ keV (Cui et al. 1997a; Dotani et al. 1997). The spectrum above 10 keV becomes much softer than in the hard state, with a variable photon index, $\Gamma \sim 1.9 - 2.5$ (Gierliński et al. 1997b; Cui et al. 1997a; Dotani et al. 1997).

Since Cyg X-1 spends only a small fraction of time in the soft state, this state is relatively less well studied compared to the hard state. Recent observations (e.g. Zhang et al. 1997a; Cui et al. 1997a; Dotani et al. 1997) during the state transition which occurred in the summer of 1996 resulted in several important discoveries. By combining ASM/RXTE and BATSE lightcurves, Zhang et al. (1997a) demonstrated that the total X-ray luminosity of Cyg X-1 remained practically constant during the transition. On the other hand, a comparison of the characteristic temperature and luminosity of the ultrasoft blackbody component before and during the transition showed that the apparent inner radius of the thin disk was at least ~ 3 times larger in the low state that in the soft state. The authors concluded that the change in the spectrum reflects a change in the relative importance of the energy release in the hot and cold regions of the flow, without a significant variation in the mass accretion rate. (Note that in a later paper, Zhang, Cui & Chen (1997b) proposed that the change in the inner radius of the disk may result from a temporary change between a prograde and retrograde disk around a rotating black hole.)

The temporal properties of Cyg X-1 during the 1996 spectral state transition (Cui et al. 1997c) also showed strong evolution. Cui et al. discovered that the observed time lag between the soft and hard energy bands is roughly ~ 10 times smaller in the soft state than in the hard state. If this time lag is due to Compton scattering of soft disk photons in the hot "corona", its magnitude must be strongly correlated with the optical depth of the hot region. The authors conclude that their result requires the presence of a larger hot "corona" in the hard state than in the soft state. Cui et al. (1997c) also argue that the observed change in the shape of the power density spectrum strongly supports this interpretation.

The results outlined above fit in very well with the predictions of the EMN model for the low–high state transition. In this scenario, the softening of the spectrum is due to a decrease in the transition radius $r_{\rm tr}$ between the ADAF zone and the thin disk, and therefore, a decrease in the size and optical depth of the hot ADAF. This is precisely what is seen in Cyg X-1. Moreover, the presence of the intermediate state, during which $r_{\rm tr}$ changed from its large low state to its small high state value, was clearly inferred both from the spectral and temporal evolution of the system (Cui et al. 1997a, 1997c; Belloni et al. 1996).

In Figure 4 we show combined PCA/HEXTE spectra taken on 1996 May 22, roughly 10 days after the onset of the hard–soft state transition (Cui et al. 1997a), together with our intermediate model spectrum modified to take into account interstellar absorption.

As in fitting the low state spectrum above, we used a grid of models constructed by varying $r_{\rm tr}$, while keeping $m = 9$ and $i = 40°$. The best fit to the data was found with $N_H = 2.7 \times 10^{22}$ cm^{-2} and $r_{\rm tr} = 3.5$. The overall agreement between the model spectrum and the data is fairly good. Our calculation reproduces both the characteristic temperature of the soft disk emission and the shape of the power-law component. The only obvious discrepancy occurs in the vicinity of Fe Kα line. As in the case of the low state, the predicted line strength is too small, and it is clear that more detailed modeling of both the ADAF and the thin disk is necessary in order to accurately reproduce the observed line emission. Though the fitted value of $r_{\rm tr}$ is very close to the marginal stable orbit, the model requires that Cyg X-1 was still in the intermediate state, consistent with the conclusions of Cui et al. (1997a, N.B. the authors use the term "settling period" instead of intermediate state) and Belloni et al. (1996).

Did Cyg X-1 reach the "true" high state during its 1996 state transition? Cui et al. (1997a, 1997c) argued that it did, based on the fact that the shape of the power density spectra observed between June and August of 1996 are very similar to those seen in Nova Muscae in its high state (Miyamoto et al. 1993). In the context of the EMN model, this implies that during the low–high state transition $r_{\rm tr}$ decreased all the way from its value in the low state (~ 100, see §3.1) to the marginally stable orbit in the high state, when the ADAF was confined to the corona above the disk.

To illustrate that this scenario captures the essential spectral features of the Cyg X-1 state transition, we use the combined simultaneous ASM/RXTE (1.3-12 keV) and BATSE/CGRO (20-600 keV) spectra of Cyg X-1 taken between April and October 1996. Each spectrum is averaged over a single CGRO spacecraft pointing period (1-3 weeks), except for a few very short pointings, for which the data from two nearby periods are combined. The ASM data points are converted to fluxes by comparing the count rates with the average ASM Crab Nebula count rates in each channel. The BATSE spectra are deconvolved by assuming the simplest spectral model, namely a power-law with an exponential cutoff. In Figure 5(a) we plot the spectra taken during the first half of the observation period, i.e. they should represent the transition from the low to the high state. The spectra taken during the subsequent high–low transition are shown in Figure 5(b). For comparison, our intermediate state spectra, computed by setting $m = 9$, $\dot{m} = \dot{m}_{\rm crit} \sim 0.11 - 0.12$ and varying $r_{\rm tr}$ from 100 to 3.2, and a high state spectrum with $r_{\rm tr} = 3$, are plotted in Figure 5(c).

By comparing the three panels in Figure 5, one can see the remarkable similarity between the data and the EMN model. Our sequence of intermediate and high state spectra clearly shows the three main characteristics of the observed spectral evolution of Cyg X-1.

(1) The softening of the spectral slope above 10 keV is very well reproduced by the model, which gives $\Gamma \sim 1.5$ for the hardest spectrum and $\Gamma \sim 2.3$ for the softest.

(2) The model spectra clearly show the anti-correlation between the fluxes in the soft and hard X-ray bands. Moreover, the relative normalization of the ultrasoft blackbody and the power-law component is very close to what is observed.

(3) According to the model, the bolometric luminosity changes by only $\sim 50\%$ during the entire sequence. This is in excellent agreement with the observations (Zhang et al. 1997a).

(4) Finally, we clearly reproduce the characteristic spectral pivoting around ~ 10 keV.

In the EMN model, the low–high state transition is triggered by a slight increase of the mass accretion rate in the system. For transient BHXBs, the change in $\dot{m}$ is most likely due to a thermal instability in the outer thin disk (e.g. Hameury et al. 1997). What causes the increase in the mass accretion rate in Cyg X-1? Disk instability is again a possible solution. However, if $\dot{m} \sim \dot{m}_{\rm crit}$ in the low state (as we have assumed in our discussion above), we need very small changes in $\dot{m}$ to cause a significant change in $r_{\rm tr}$. For instance the difference between the values of $\dot{m}$ in the hardest and softest states in Figure 5c is only $\sim 15\%$. Since in Cyg X-1, the mass transfer is powered by a wind from the supergiant companion star (Gies & Bolton 1986b), fluctuations in $\dot{m}$ on the level of a few tens of percent are not improbable.

4. GRO J0422+32

The transient source GRO J0422+32 was discovered in outburst by BATSE/CGRO on August 4 1992 and reached its maximum luminosity in the 40-150 keV range by August 8 (Paciesas et al. 1992). Its fast rise was followed by an exponential decay with a characteristic time scale ~ 40 days, a secondary maximum ~ 140 days after the onset of the initial outburst (e.g. Harmon et al. 1992, 1994), and a steepening of the decay after about 230 days. The overall light curve resembled closely those of typical transient sources like Nova Muscae, GS 2000-25 and A0620-00 (Tanaka & Shibazaki 1996 and references therein).

GRO J0422+32 was observed at various times during the first few months of the outburst by ASCA (Tanaka 1993), ROSAT (Pietsch et al. 1993), Mir/TTM (Sunyaev et al. 1993), and OSSE (Grove et al. 1997). Its X-ray spectrum in all cases was hard and reasonably well-fitted by an exponentially truncated power-law, similar to Cyg X-1 in its low state. An interesting characteristic of this transient is a complete absence of an ultrasoft

component during the outburst, similar to another X-ray Nova, GS 2023-338 (Sunyaev et al. 1993). The peak luminosity in 2-300 keV is estimated to be $\sim 5 \times 10^{37}$ erg s^{-1} (Sunyaev et al. 1993 scaled for $d = 2.6$ kpc, see §4.1), which corresponds to $\sim 0.05 L_{\rm Edd}$ for an accreting object of mass $m = 9$ (see §4.1).

4.1. Binary Parameters

An optical counterpart of GRO J0422+32 with peak magnitude $V \sim 13.2$ was identified by Castro-Tirado et al. (1993). Follow-up observations showed that in quiescence the source dropped down to $V = 22.4$ (Zhao et al. 1994), representing a change of over 9 magnitudes. Further study revealed that the system is a low-mass binary with an orbital period $P = 5.0$ hours and a mass function $f(M) = 1.21 M_\odot$ (Filippenko, Matheson & Ho 1995; Casares et al. 1995a; Chevalier & Ilovaisky 1996).

The optical spectrum during quiescence shows the secondary to be a normal M2 dwarf with a mass $\sim 0.39 M_\odot$ (Filippenko et al. 1995; Casares et al. 1995b). The inclination of the system is highly uncertain. Filippenko et al. (1995) derived $i = 48^\circ$ from a study of the Hα emission line, which gives a black hole mass $M = 3.6 M_\odot$. Kato, Mineshige & Hirata (1995) claimed to have detected an eclipse feature in the orbital lightcurve, implying that the binary is close to being edge-on. Recently, however, Beekman et al. (1997) studied the flux variation due to the distortion of the secondary and concluded that $13^\circ \leq i \leq 31^\circ$, assuming that 30% of the light in the I-band comes from the accretion disk (Filippenko et al. 1995). This result implies that the black hole mass has a lower limit of $\sim 9 M_\odot$, which is much higher than previously thought. In what follows we will adopt $m = 9$.

The distance to the binary can be calculated using the method described by Barret, McClintock & Grindlay (1996, the authors identify it as "method I"), in which they derive the absolute magnitude of the secondary and compare it to the apparent de-reddened magnitude in quiescence. The luminosity of the secondary is estimated using its known spectral type, which can be converted into a visual flux (Popper 1980), assuming that the radius of the star is equal to the average Roche lobe radius (Paczyński 1971). We obtain $d \simeq 2.6$ kpc. (This number is different from that quoted by Barret et al. [1996] since they used a different visual extinction value; here we adopt $A_V = 1.2$ [Filippenko et al. 1995]). Note that this result does not depend on the mass of the black hole or the inclination of the system; the only relevant parameters are mass and spectral type of the secondary, and its apparent visual magnitude. Because of this, we feel that our distance estimate is quite robust.

4.2. Outburst Spectrum

The relatively low peak luminosity, the absence of a soft component, and the general similarity of the spectrum of GRO J0422+32 to the low state of Cyg X-1 (Sunyaev et al. 1993), lead us to propose that at the peak of its outburst this system was in the low spectral state, as described in §2.2. In our scenario, the rapid rise and decline of the X-ray luminosity occurred through a dramatic change in the mass accretion rate, caused perhaps by an instability in the outer thin disk (e.g. Cannizzo 1993; Hameury et al. 1997). However, since the spectrum of the system remained hard, and none of the published spectra show any indication of the Compton reflection component or iron fluorescence (e.g. see Figure 6), we conclude that the transition radius between the hot and cold emission regions was at all times greater than $\sim 100 R_{\rm Schw}$, and that the mass accretion rate remained at or below its critical value, $\dot{m}_{\rm crit} \sim 0.1$. Thus, this outburst of GRO J0422+32 is significantly different from that of Nova Muscae 1991, in which the accretion rate apparently reached the Eddington limit and the system went from the quiescent to the very high spectral state (EMN). In GRO J0422+32, the transition occurred between the quiescent and low spectral states.

In Figure 6 we plot a combined TTM (2-20 keV), HEXE (20-200 keV, from Sunyaev et al. 1993 and Maisack et al. 1993) and OSSE (50-600 keV, from Grove et al. 1997) spectrum of GRO J0422+32 taken three weeks after the X-ray peak of the outburst (1992 August 29 – September 2). This period corresponds to approximately half maximum intensity at 100 keV. Grove et al. fitted this data using an exponentially truncated power-law model, and obtained a best fit photon index of 1.5 and e-folding energy of ~ 130 keV. Superimposed on the data are our model spectra calculated for $m = 9$, $\alpha = 0.3$, $\beta = 0.5$, $\dot{m} = 0.1$ and values of i ranging from 15° to 75°, as shown in the figure. We adopted $r_{\rm tr} = 10^4$, but the results are the same for other values of $r_{\rm tr}$ down to 10^2.

All three model spectra shown in Figure 6 reproduce the observed spectral slope very well, though to fit the shape of the exponential cut-off we need $i \gtrsim 40°$. Moreover, the spectrum computed with $i = 45°$ gives the correct normalization (assuming d=2.6 kpc) as well as spectral shape. The binary parameters discussed in §4.1 require that, for a $9 M_\odot$ black hole, the system inclination must be around 31°. The discrepancy between this value and our estimate of 45° highlights some of the limitations of the model (see the discussion in §3.1).

4.3. E-folding Energy vs. Luminosity

OSSE observed GRO J0422+32 for 33 days from the peak of the outburst. Throughout this period the spectrum was well described by an exponentially truncated power-law. However, Grove et al. (1997) found that the best fit model parameters underwent a substantial evolution. In particular, as the hard X-ray luminosity declined with time, the e-folding energy increased nearly monotonically, i.e. the two parameters were anti-correlated. The nearly linear relation between these two parameters is shown in Figure 7. This result is in good agreement with what is expected in the low spectral state (see Figure 2 and the discussion in §2.3). If, as we have assumed, the mass accretion rate in GRO J0422+32 at the peak of the outburst is near its critical value, and the decline of the hard X-ray flux is a result of a decrease in $\dot{m}$, the temperature of the hot flow must be anti-correlated with luminosity (the segment between low state and quiescent state in Figure 2).

One must keep in mind, however, that a detailed comparison between Figures 2 and 7 is difficult. The e-folding energies plotted in Figure 7 were obtained by fixing the photon index of the spectra to $\Gamma = 1.5$, which is the best fit value for the combined spectrum shown in Figure 6. This was done because the OSSE data do not extend to low enough energies to allow a meaningful fit of both E_f and Γ. It is not clear from the data whether the photon index changed during the period when the system was observed. On the other hand, our model predicts a 15% change in the spectral slope during this period, with the hardest spectra near the outburst maximum. Though this discrepancy would not affect the overall qualitative nature of our result, it would undoubtedly change the exact values of E_f for a given luminosity. Moreover, the numerical values for the gas temperature plotted in Figure 2 do not exactly correspond to the e-folding energy of the observed spectrum (though we expect the two to be proportional to each other), since E_f is in a sense a measure of the *average* electron temperature in the ADAF.

5. GRO J1716−24

The transient system GRO J1719−24 was discovered in outburst on 1993 September 25 by BATSE and SIGMA (Harmon et al. 1993; Ballet et al. 1993). The hard X-ray flux (20-100 keV) reached its maximum of ~ 1.4 Crab (e.g. van der Hooft 1996) five days after the original detection, and for the next 70 days the flux level remained high, declining by no more than $\sim 20\%$. This was followed by an abrupt drop, during which the source flux dipped below the BATSE 1 day detection limit of 0.1 Crab. For the next ~ 200 days the flux level remained undetectable by BATSE. However, between September 1994 and September 1995, the light curve of the source exhibited five separate flare events, with

maximum amplitude roughly 1/3 of the original outburst (e.g. Hjellming et al. 1996). These secondary flares were characterized by slow, almost linear rises and abrupt decays, opposite to what is typically observed in X-ray novae (e.g. see a review by Tanaka & Shibazaki 1996).

The optical counterpart for GRO J1719−24 was found by Della Valle, Mirabele & Cordier (1993). From the interstellar absorption, Della Valle, Mirabele & Rodriuez (1994) estimated the distance to be ~ 2.4 kpc, which together with the upper limit on the brightness of the system in quiescence, allowed them to conclude that the companion is a main-sequence star of spectral type later than K. Interpreting the prominent optical period of $14^{\rm h}.7$ as a superhump phenomenon, Masetti et al. (1996) estimated that the mass of the compact object must be $M > 4.6 M_{\odot}$. Thus, GRO J1719−24 appears to be a low-mass black hole system.

On September 25-26 1993 the source spectrum was hard, similar to the low state of Cyg X-1, with a power-law photon index $\Gamma = 2.0$ in the hard X-ray (20-100 keV) band, and $\Gamma = 1.6$ in the softer (2-27 keV) band (Harmon et al. 1993; Kaniovsky, Borozdin, & Sunyaev 1993). Van der Hooft et al. (1996) report that the 20-100 keV spectrum softened to $\Gamma = 2.3$ during the rise to the first maximum and continued to soften gradually thereafter.

The spectral behavior of GRO J1719−24 during the secondary flares (as we will denote the five smaller events to distinguish them from the original outburst) in 1994-95 is rather uncertain. OSSE observations at the trailing edge of the first flare (1994 November $9 - 14$) showed a power-law spectrum with no high energy cut-off and photon index $\Gamma \sim 2.4$ (Grove et al. 1997). The same team observed a hard exponentially truncated power-law spectrum with $\Gamma \sim 1.5$ near the peak of the second flare (1995 February 1-14). Just two days later, the source was detected by the MIR/Kvant team, who reported a power-law spectrum (in the energy band 2-27 keV) with a photon index 2.1 ± 0.3.

To summarize, it appears that GRO J1719−24 was observed in three distinct spectral states, two of which are similar to the soft and hard states of Cyg X-1. When the source was bright in the hard X-ray band during the flares, its spectrum was best characterized as a hard power-law with an exponential cut-off at $\sim 100 - 130$ keV (low state), while the periods of lower hard X-ray flux during the flares seemed to be associated with the appearance of a steeper power-law component with $\Gamma > 2.0$ and no cut-off below ~ 500 keV (high state). The third spectral state appeared during the first and largest outburst, and is characterized by high hard X-ray flux and a rather soft spectrum with $\Gamma \lesssim 2.3$, reminiscent of the very high state seen in Nova Muscae and GX 339−4 (e.g. Ebisawa et al. 1994; Miyamoto et al. 1991).

How can this behavior be interpreted in terms of the EMN spectral state model? Since the rise to peak intensity during the first outburst was very similar to the outbursts exhibited by other black hole transients (e.g. Nova Muscae, A0620-00), we speculate that during this time the system made a rapid transition from the quiescent to the very high spectral state, following a dramatic increase in the mass accretion rate. The 20–100 keV flux from GRO J1719−24 peaked at roughly $\sim 0.4\,\mathrm{phot\,cm^{-2}\,s^{-1}}$ (van der Hooft et al. 1996), which corresponds to $\sim 1.5 \times 10^{37}\,\mathrm{erg\,s^{-1}}$ (for a source with a photon index $\Gamma = 2.3$ at a distance of 2.4 kpc), comparable to the luminosity of Nova Muscae in the very high state (Ebisawa et al. 1994; EMN). The rapid drop in the hard X-ray flux ~ 70 days after the peak luminosity, is also very similar to that seen in the lightcurve of Nova Muscae (EMN), and we interpret it as the transition from the very high to the high state. After that, the hard X-ray flux remained below the BATSE threshold until the accretion rate dropped low enough for an ADAF to form, i.e. the system entered an intermediate state and moved into the low state.

The most straight-forward interpretation of the data during the secondary flares directly follows from Grove et al. (1997). At the time of flare maxima, the system was in the low (or perhaps intermediate) spectral state, characterized by a hard power-law spectrum with a thermal cut-off. Unfortunately, the data are not good enough to place constraints on the presence of the Compton reflection component, so that the position of the transition radius is uncertain, though it is likely that $r_{\rm tr} \gtrsim 30$. We propose that the rapid decay which accompanied each secondary flare was caused by an increase in $\dot{m}$ which precipitated a corresponding decrease in $r_{\rm tr}$, or a disk instability of some sort which caused $r_{\rm tr}$ to decrease suddenly. Thus, during the times when the flux in the BATSE band was low, we propose that the system was in the high spectral state, with $r_{\rm tr}$ close to the last stable orbit.

In Figure 8 we plot the e-folding energy obtained from the OSSE data taken on 1995 February 1-14 near the peak of the second flare, against the integrated OSSE flux. During this time, the X-ray luminosity was decreasing nearly monotonically with time. As in Figure 6, the values of E_f were derived using an exponentially truncated power-law model with a fixed photon index, $\Gamma = 1.5$. We see that the hard X-ray luminosity and the e-folding energy are correlated. A comparison with Figure 2 shows that this behavior is expected if the system is in the intermediate state and is switching from the low to the high state. Thus, the data in Figure 8 confirms the proposal we have made for the secondary flares.

A detailed comparison of Figures 7 and 8 shows that the values of E_f in GRO J1719−24 are somewhat higher compared to GRO J0422+32. According to the model, the minimum E_f in Figure 7 must be roughly equal to the maximum E_f in Figure 8 (see Figure

2). Instead the latter appears to exceed the former by ~ 30 keV, though the errorbars are large. If this result is real it might imply that GRO J1719−24 has smaller inclination, or perhaps larger black hole spin.

Since during the high spectral state most of the system luminosity comes out as ultrasoft blackbody disk emission, observations in the energy range below 10 keV would provide the most direct test of our interpretation of the data on GRO J1719−24. Unfortunately, we are not aware of any such observations made during the times when the source was "off" in the BATSE energy band. According to our interpretation, the system should have been in the high state and, therefore, very bright around 1 keV.

In conclusion, we emphasize that the behavior of GRO J1719−24 is qualitatively quite similar to that of Nova Muscae 1991. Both sources showed a rapid increase in the 20-100 keV flux, followed by an abrupt drop, and followed later by a secondary maximum. However, there are two important differences between the lightcurves of the two systems. Firstly, the complete outburst in GRO J1719−24 lasted at least twice as long as that in Nova Muscae, indicating that the time scale for the decrease of the mass accretion rate was different in the two systems. Secondly, GRO J1719−24 showed five secondary flares, instead of just one observed in Nova Muscae. According to our interpretation, these flares were caused by oscillations of the transition radius, either as a result of fluctuations in the mass accretion rate or because of a disk instability. Nova Muscae, perhaps because of the mare rapid decline of $\dot{m}$, did not undergo such oscillations.

6. Conclusions

The ADAF solution (Ichimaru 1977; Rees et al. 1982; Narayan & Yi 1994, 1995b; Abramowicz et al. 1995; Chen et al. 1995) is currently the only known stable accretion model that explains the observed X-ray spectra of BHXBs with a self-consistent treatment of gas dynamics and radiative transfer. The model satisfies mass and momentum conservation at each radius, solves for the electron and ion temperatures through the use of appropriate energy equations, and includes a fairly sophisticated treatment of radiative processes. Narayan (1996) and EMN used the ADAF solution to develop a unified picture of the quiescent, low, intermediate and high spectral states observed in BHXBs. In their model, the accretion flow consists of two distinct parts, a hot ADAF inside some transition radius $r_{\rm tr}$ (in Schwarzschild units), and a standard thin disk with a hot corona outside $r_{\rm tr}$. The different spectral states then correspond to different values of the two main parameters, $\dot{m}$ and $r_{\rm tr}$.

The basic scenario that emerged from the work of Narayan (1996) and EMN is summarized in §2. In the quiescent and low spectral states the transition radius is relatively large, $r_{\rm tr} \gtrsim 100$, and variations in the observed spectrum result solely from changes in the mass accretion rate, $\dot{m}$. In the quiescent state, we have $\dot{m} < 10^{-3}$, while in the low state $\dot{m}$ can be as high as about 0.1 (in Eddington units). The low state survives only until $\dot{m}$ reaches a critical value $\dot{m}_{\rm crit} \sim 0.1$. When $\dot{m} > \dot{m}_{\rm crit}$, the outer parts of the ADAF can no longer be in thermal equilibrium and the cool disk begins to encroach into the ADAF. When the transition radius lies between $r_{\rm tr} \sim 100$ and 3 (with $\dot{m} \sim \dot{m}_{\rm crit}$) we have the so-called intermediate state. Finally, above a certain $\dot{m}$, $r_{\rm tr}$ comes down to the marginally stable orbit, $r_{\rm tr} = 3$, and the ADAF is restricted to a corona above the disk. This is the high state.

Some of the basic features of the EMN model are similar to other models that have appeared previously in the literature. Shapiro et al. (1976) and Ichimaru (1977) suggested that the low state of Cyg X-1 correspond to an optically thin, hot accretion flow, rather than the standard thin disk. Ichimaru further speculated that the transition between the hard and soft states in Cyg X-1 might be caused by a change in the outer boundary conditions of the accretion flow, which determines whether the accreting gas assumes the standard thin disk configuration or forms a hot optically thin flow. However, the model proposed by EMN is the first successful attempt to unify the quiescent, low, intermediate and high spectral states within the framework of a single self-consistent calculation (see Figure 1).

Application of the model outlined above to the outburst of Nova Muscae 1991 (EMN) demonstrated that it reproduces well the individual low, intermediate and high state spectra of this system. Moreover, the theoretical light curve based on a simple mapping between the mass accretion rate, transition radius and time is in good agreement with the observed X-ray and γ-ray light curves. Further confirmation of the main results of EMN came from more detailed analysis of the spectra of Nova Muscae observed while the system was in the intermediate state (Życki et al. 1997). From detailed fitting of the Fe Kα emission, Życki et al. concluded that the inner edge of the thin disk did increase during this period, as predicted by EMN. Życki et al. also showed that there is a discrepancy in the exact value of $r_{\rm tr}$ during the intermediate state, but this is not a serious problem, as we have argued in §2.2.

The present paper describes further tests of the EMN model on other black hole systems. In §3 we analyze data taken during the 1996 hard–soft state transition of Cyg X-1 and compare with the predictions of the model. The results are encouraging. The hard and soft spectra of Cyg X-1 are reasonably well fitted by low state and intermediate state

model spectra (Figures 3 and 4). The best fit value of the transition radius for the hard state is $r_{\rm tr} \sim 100$, consistent with the narrow width of the iron fluorescence line observed by Ebisawa et al. (1996) in the low state. The spectrum corresponding to $r_{\rm tr} = 30$ is somewhat too soft to reproduce the data, though we feel that the uncertainties in our model (e.g. use of Newtonian dynamics and radiative transfer, as well as a simplistic treatment of the flattening of the ADAF density profile) are comparable to the difference between those two curves. We would thus say that the low state in Cyg X-1 is consistent with any $r_{\rm tr} \gtrsim 20$. The soft state spectrum is best described by a model with $r_{\rm tr} \sim 3.5$, i.e. close to the marginally stable orbit.

We have also compared a sequence of intermediate and high state spectra computed for several values of $r_{\rm tr}$ between 100 (its value in the low state) and 3 (the marginally stable orbit for a non-rotating black hole), to observations made by BATSE and RXTE/ASM during the 1996 transition in Cyg X-1. From Figure 5, it is clear that in addition to explaining the broad qualitative features of the transition, the model reproduces very well several details seen in the observations. The range of photon indices obtained with the model, $\Gamma \sim 1.5 - 2.3$, is very similar to that seen in the data. The model and the data both show anti-correlation between the soft and hard X-ray flux. The model also reproduces the pivoting around 10 keV seen in the data as well as the nearly constant bolometric luminosity throughout the transition. The striking similarity between the model and observations indicates that the general picture (Narayan 1996, EMN) in which the low–high state transition arises from a change in the transition radius (perhaps as a result of a minor fluctuation in the mass accretion rate) must be close to the truth.

In §2.3 we review the main spectral signatures of the state transitions predicted by the EMN model, and discuss how they can be used to deduce the physical changes in the accretion flow that accompany such transitions. We show that in both the low state and in the intermediate state a decrease in hard X-ray luminosity must invariably be accompanied by a softening of the overall spectrum. Thus, from the point of view of an observer, if all one has is hard X-ray data, it is difficult to distinguish between a decrease of $\dot{m}$ in the low state and a decrease in $r_{\rm tr}$ in the intermediate state. We show, however, that the position of the high energy cut-off is a much better diagnostic. In the low state, the e-folding energy and the hard X-ray luminosity are anti-correlated, since at lower mass accretion rates the ADAF is hotter. The exact opposite happens in the intermediate state, where a decrease in $r_{\rm tr}$ causes both the hard X-ray flux and the temperature of the hot flow to drop. The two effects are illustrated in Figure 2. To show how these properties of the model could be exploited in interpreting observations of real systems, in §§4 and 5 we discuss the transient systems GRO J0422+32 and GRO J1719−24.

We find that the observed spectral evolution of GRO J0422+32 after the peak of its 1992 outburst must have corresponded to a transition between the low and quiescent spectral states. This interpretation arises from the fact that the cut-off temperature was anti-correlated with the X-ray luminosity during the first 30 days of the decline when OSSE observed the source (Figure 7). Moreover, we find that the spectrum observed at roughly half maximum luminosity is very well fitted by a low state model spectrum computed with $m = 9$, and $r_{\rm tr} = 10^4$. Thus, GRO J0422+32 seems to have been very different from a more "typical" transient like Nova Muscae or A0620−00. In GRO J0422+32 it would appear that the mass accretion rate even at the peak of the outburst was at or below the critical rate $\dot{m}_{\rm crit}$, i.e. $\dot{M} \lesssim 0.1\dot{M}_{\rm Edd}$. Thus, GRO J0422+32 was dominated by an ADAF all through its outburst. Interestingly, the accretion rate in this system in quiescence is estimated at $\dot{m} \sim 10^{-4}$ (Menou 1997, private communication), significantly lower than quiescent values in other transient systems (Narayan et al. 1996, 1997a).

On the other hand, the outburst of GRO J1719−24 appears to have been closer to that of Nova Muscae. We make a tentative proposal that the first and largest peak corresponds to a transition from the quiescent to the very high state, characterized by high X-ray luminosity and a power-law spectrum with photon index $\gtrsim 2.3$ (Hooft et al. 1996). The sharp drop in the BATSE flux two month after the initial outburst is very similar to that observed in Nova Muscae, which EMN identified as the transition from the very high to the high state. According to our proposal, the secondary flares correspond to a series of transitions between the high and intermediate spectral states. Both the shapes of the spectra and the observed correlation between the e-folding energy and X-ray flux support this interpretation. Of course, the fact that GRO J1719−24 oscillated five times between the high and intermediate state differentiates this source from Nova Muscae and A0620−00 which had only one such transition. Perhaps the decline of $\dot{m}$ was not monotonic in GRO J1719−24, or more likely the outer thin disk underwent some kind of a disk instability.

Although we have been quite successful in applying the EMN model to Cyg X-1, GRO J0422+32 and GRO J1719−24, we would like to emphasize that the main results presented in this paper are still somewhat qualitative, and the uncertainties in the model are still too large to draw meaningful quantitative conclusions. The accretion flow calculations employed here take into account most of the relevant physical processes in a self-consistent way, and are superior to other analyses in the literature. Nevertheless, a number of improvements need to be made before we can attempt detailed comparisons between our models and the observational data.

The main avenue of future work lies in incorporating relativistic effects into the calculations. Relativistic global flow solutions in Kerr geometry (Abramowicz et al. 1996;

Peitz & Appl 1997; Gammie & Popham 1997) and gravitational redshift have already been used in modeling the spectrum of Sgr A* (Narayan et al. 1997d). In calculating radiative transfer in an ADAF, we need to include the effects of ray bending and Doppler boosts due to the motion of the gas (Jaroszynski & Kurpiewski 1997), and to modify our treatment of Compton scattering to take into account the bulk radial motion of the gas (Titarchuk et al. 1996, 1997). Our treatment of the thin disk spectrum must also be modified to include relativistic effects. The strength and shape of the iron fluorescence line and the corresponding absorption edge have recently been used as a successful diagnostic to probe the geometry and physical characteristics of the accretion flow (e.g. Życki et al. 1997; Cui et al. 1997b). However, in order to use these features to constrain our model we must assume a more realistic density profile of the ADAF in the vertical direction, instead of truncating the flow near the poles. We also need to compute self-consistently the ionization state of the thin disk.

We thank M. Gierliński for providing Cyg X-1 low state data, and J. Nevelainen, T. Aldcroft and J. McClintock for their help with XSPEC. This work was supported in part by NSF grant AST 9423209 and NASA grant NAG 5-2837. A. A. E. was supported by a National Science Foundation Graduate Research Fellowship.

REFERENCES

Abramowicz, M. A., Chen, X., Grantham, M., Lasota, J.-P. 1996, ApJ, 471, 762

Abramowicz, M. A., Chen, X., Kato, S., Lasota, J. P., & Regev, O. 1995, ApJ, 438, L37

Ballet, J., Denis, M., Gilfanov, M., & Sunyaev, R. 1993, IAU Circ. 5874

Balucinska-Church, M., Belloni, T., Church, M. J., Hasinger, G. 1995, A&A, 302, L5

Barr, P., White, N. E., Page, C. G. 1985, MNRAS, 216, 65

Barret, D, McClintock, J. E. & Grindlay, J. E. 1996, ApJ, 473, 963

Beekman, G., Shahbaz, T., Naylor, T., Charles, P. A., Wagner, R. M., & Martini, P. 1997, MNRAS, 290, 303

Belloni, T., Mendez, M., van der Klis, M., Hasinger, G., Lewin, W. H. G., van Paradijs, J. 1996, ApJ, 472, L107

Bisnovatyi-Kogan, G. S. & Lovelace, R. V. E. 1997, ApJ, 486, 43

Blackman 1997, submitted to Phys Rev Let

Bowyer, S., Byram, E. T., Chubb, T. A., Friedman, M. 1965, Science, 147, 394

Bregman, J., Butler, D., Kemper, E., Koski, A., Kraft R. P., Stone, R. P. S. 1973, ApJ, 185, L117

Cannizzo, J. K. 1993, in Accretion Disks in Compact Stellar Systems, ed. J. C. Wheeler, Singapore: World Scientific Publishing, 6

Casares, H., Marsh, T. R., Charles, P. A., Martin, A. C., Martin, E. L., Harlaftis, E. T., Pavlenko, E. P., Wagner, R. M. 1995a, MNRAS, 274, 565

Casares, H., Martin, A. C., Charles, P. A., Martin, E. L., Rebolo, R., Harlaftis, E. T., Castro-Tirado, A. J. 1995b, MNRAS, 276, L35

Castro-Tirado, A. J., Pavlenko, E. P., Shlyapnikov, A. A., Brandt, S., Lund, N., Ortiz, J. L. 1993, A&A, 276, L37

Chen, X. 1995, MNRAS, 275, 641

Chen, X., Abramowicz, M. A., Lasota, J. P., Narayan, R., Yi, I. 1995, ApJ, 443, L61

Chevalier, C. & Ilovaisky, S. 1996, A&A, 312, 105

Cui, W., Heindl, W. A., Rothschild, R. E., Zhang, S. N., Jahoda, K., Focke, W. 1997a, ApJ, 474, L57

Cui, W., Ebisawa, K., Dotani, T., & Kubota, A. 1997b, ApJL, in press

Cui, W., Zhang, S. N., Focke, W., Swank, J. H. 1997c, ApJ, 484, 383

Della Valle, M., Mirabele, F., & Cordier, B. 1993, IAU Circ. 5876

Della Valle, M., Mirabele, I. F. & Rodriuez, L. F. 1994, A&A, 290, 803

Dolan, J. F. 1992, ApJ, 384, 249

Done, C., Mulchaey, J. S., Mushotzky, R. F., Arnaud, K. A. 1992, ApJ, 395, 275

Dotani, T. et al. 1997, ApJ, 485, L87

Dove, J. B., Wilms, J., Maisack, M., Begelman, M. C. 1997a, ApJ, 487, 759

Dove, J. B., Wilms, J., Nowak, M. A., Vaughan, B. A., & Begelman, M. C. 1997b, submitted to ApJLetters

Ebisawa, K. et al. 1994, PASJ, 46, 375

Ebisawa, K., Titarchuk, L., & Chakrabarti, S. K. 1996, PASJ, 48, 59

Ebisawa, K., Ueda, Y., Inoue, H., Tanaka, Y., White, N. E. 1996, ApJ, 467, 419

Esin, A. A., McClintock, J. E., & Narayan, R. 1997, ApJ, 489, 000

Fabian, A. C., Rees, M. J., Stella, L., White, N. E. 1989, MNRAS, 238, 729

Filippenko, A. V., Matheson, T., Ho, L. C. 1995, ApJ, 455, 614

Frank, J., King, A., & Raine, D. 1992, Accretion Power in Astrophysics (Cambridge, UK: Cambridge University press)

Gammie, C. & Popham, R. 1997, ApJ, in press

George, I. M. & Fabian, A. C. 1991, MNRAS, 249, 352

Gierliński, M., Zdziarski, A. A., Done, C., Johnson, W. N., Ebisawa, K., Ueda, Y., Haardt, F., Phlips, B. F. 1997a, MNRAS, 288, 958

Gierliński, M., Zdziarski, A. A., Dotani, T., Ebisawa, K., Jahoda, K., Johnson W. N. 1997b, in Proceedings of 4th Compton Symposium, in press

Gies, D. R. & Bolton, C. T. 1986a, ApJ, 304, 371

Gies, D. R. & Bolton, C. T. 1986b, ApJ, 304, 389

Gies, D. R. & Bolton, C. T. 1982, ApJ, 260, 240

Gilfanov, M. et al. 1993, A&A Suppl. Ser., 97, 303

Grove, J. E., Johnson, Kroeger, R. A., McNaron-Brown, K., Skibo, J. G., & Phlips, B. F. 1997, submitted to ApJ

Gruzinov 1997, submitted to ApJ

Haardt, F., Done, C., Matt, G., Fabian, A. C. 1993, ApJ, 411, L95

Hameury, J.-M., Lasota, J.-P., McClintock, J. E., & Narayan, R. 1997, 489, 234

Harmon, B. A. et al. 1992, IAU Circ. 5685

Harmon, B. A., Zhang, S. N., Paciesas, W. S., & Fishman, G. J. 1993, IAU Circ. 5874

Harmon, B. A. et al. 1994, in the Second Compton Symposium, eds. C. E. Fichtel, N. Gehrels, & J. P. Norris (AIP, New York), p. 210

Hawley, J. F. & Balbus, S. A. 1996, in Physics of Accretion Disks, eds. S. Kato et al., Gordon and Breach Sci. Publ., 273

Herrero, A., Kudritzki, Gabler, R., Vilchez, J. M., Gabler, A. 1995, A&A, 297, 556

Hjellming, R. M., Rupen, M. P., Shrader, C. R., Campbell-Wilson, D., Hunstead, R. W., & McKay, D. J. 1996, ApJ, 470, L105

Huang, M. & Wheeler, J. C. 1989, ApJ, 343, 229

Ichimaru, S. 1977, ApJ, 214, 840

Jaroszyński, M. & Kurpiewski, A. 1997, A&A, 326, 419

Kaniovsky, A., Borozdin, K., & Sunyaev, R. 1993, IAU Circ. 5878

Kato, T., Mineshige, S., & Hirata, R. 1995, PASJ, 47, 31

Lasota, J. P., Narayan, R., & Yi, I. 1996b, A&A, 314, 813

Liang, E. 1997, Phys. Rep., in press

Lightman, A. P. & White, T. R. 1988, ApJ, 335, 57

Mahadevan, R., Narayan, R., Yi, I. 1996, ApJ, 465, 327

Maisack et al. 1993, in Second Compton Symposium, eds. C. E. Fichtel, N. Gehrels, & J. P. Norris (AIP, New York), p. 304

Margon, B. & Bowyer, S. 1973, ApJ, 185, L113

Masetti, N., Bianchini, A., Bonibaker, J., Della Valle, M., & Vio, R. 1996, A&A, 314, 123

McClintock, J. E., Horne, K., & Remillard, R. A. 1995, ApJ, 442, 358

Melia, F. & Misra, R. 1993, ApJ, 411, 797

Mendez, M. & van der Klis, M. 1997, ApJ, 479, 926

Meyer, F. & Meyer-Hofmeister, E. 1994, A&A, 288, 175

Mineshige, S. 1996, PASJ, 48, 93

Mineshige, S. & Wheeler, J. C. 1989, ApJ, 343, 241

Miyamoto, S., Iga. S., Kitamoto, S., & Kamado, Y. 1993, ApJ, 403, L39

Miyamoto, S., Kimura, K., Kitamoto, S., Dotani, T., & Ebisawa, K. 1991, ApJ, 383, 784

Morrison, R. & McCammon, D. 1983, ApJ, 270, 119

Narayan, R. 1997, in Proc. IAU Colloq. 163 on Accretion Phenomena & Related Outflows, ASP Conf. Series, eds. D. T. Wickramasinghe et al., 75

Narayan, R. 1996, ApJ, 462, 136

Narayan, R., Barret, D., & McClintock, J. E. 1997a, ApJ, 482, 448

Narayan, R., Garcia, M. R. & McClintock, J. E. 1997b, ApJ, 478, 79

Narayan, R., Kato, S. & Honma, F. 1997c, ApJ, 476, 49

Narayan, R., Mahadevan, R., Grindlay, J. E., Popham, B., Gammie, C. 1997d, ApJ, 492, in press

Narayan, R., McClintock, J. E., & Yi, I. 1996, ApJ, 457, 821

Narayan, R. & Yi, I. 1994, ApJ, 428, L13

Narayan, R. & Yi, I. 1995a, ApJ, 444, 231

Narayan, R. & Yi, I. 1995b, ApJ, 452, 710

Narayan, R., Yi, I., & Mahadevan, R. 1995, Nature, 374, 623

Ninkov, Z., Walker, G. A. H., Yang, S. 1987, ApJ, 321, 425

Novikov, I. D. & Thorne, K. S. 1973, in Black Holes, ed. DeWitt, C. and B. (Gordon & Breach, NY), 343

Nowak, M. A. 1995, PASP, 107, 1207

Paciesas et al. 1992, IAU Circ. 5580

Paczyński, B. 1971, ARA&A, 9183

Peitz, J. & Appl, S. 1997, MNRAS, 286, 681

Phlips, B. F. et al. 1996, ApJ, 465, 907

Pietsch, N. et al. 1993, A&A, 273, L11

Popper, D. M. 1980, ARA&A, 18, 115

Poutanen, J., Krolik, J. H., & Ryde, F. 1997, MNRAS, in press

Quataert 1997, submitted to ApJ

Rees, M. J., Begelman, M. C., Blandford, R. D., & Phinney, E. S. 1982, Nature, 275, 17

Shakura, N. I. & Sunyaev, R. A. 1973, A&A, 24, 337

Shapiro, S. L., Lightman, A. P., & Eardley, D. M. 1976, ApJ, 204, 187 (SLE)

Shimura, T. & Takahara, F. 1995, ApJ, 445, 780

Sunyaev, R. A. et al. 1993, A&A, 280, L1

Tanaka, Y. 1993, IAU Circ. 5851 (J0422)

Tanaka, Y. & Lewin, W. H. G. 1995, X-ray Binaries, eds. W. H. G. Lewin et al., Cambridge Univ. Press., 126

Tanaka, Y. & Shibazaki, N. 1996, ARA&A, 34, 607

Titarchuk, L. G., Mastichiadis, A. & Kylafis, N. D. 1996, A&A Suppl. Ser., 120, C171

Titarchuk, L. G., Mastichiadis, A. & Kylafis, N. D. 1997, ApJ, 487, 834

van der Hooft, F. et al. 1996, ApJ, 458, L75

van der Klis, M. 1994, ApJS, 92, 511

Walborn, N. R. 1973, ApJ, 179, L123

White, T. R. Lightman, A. P. & Zdziarski, A. A. 1988, ApJ, v331, 939

Zhang, S. N., Cui, W., Harmon, B. A., Paciesas, W. S., Remillard, R. E., van Paradijs, J. 1997a, ApJ, 477, L95

Zhang, S. N., Cui, W., Chen, W. 1997b, ApJ, 482, 155

Zhao, P. et al. 1994, IAU Circ. 5929

Życki, P. T., Done, C., & Smith D. A. 1997, submitted to ApJL.

Życki, P. T., Czerny, B. 1994, MNRAS, 266, 653

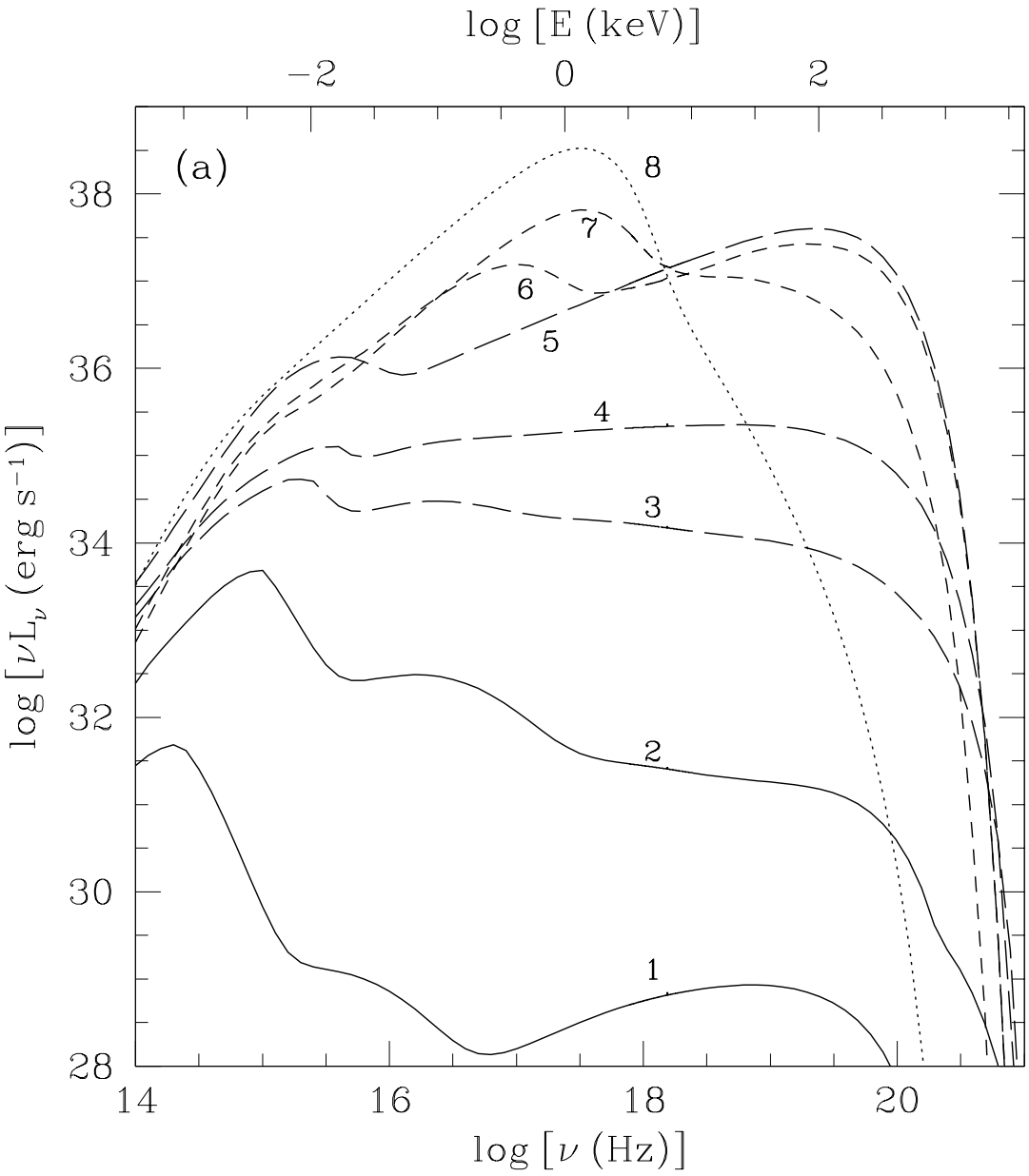

Fig. 1.— (a) A sequence of spectra corresponding to the quiescent state (solid line), low state (long-dashed line), intermediate state (short-dashed line), and high state (dotted line), computed with $m = 9$, $i = 40°$, $\alpha = 0.3$, $\beta = 0.5$, and the following values of $\log(r_{\rm tr})$ and $\dot{m}$: (a) 1–(3.9, 10^{-4}); 2–(3.9, 10^{-3}); 3–(3.9, 0.01); 4–(3.9, 0.03); 5–(3.9, 0.11); 6–(1.5, 0.11); 7–(0.5, 0.12); 8–(0.5, 0.4).

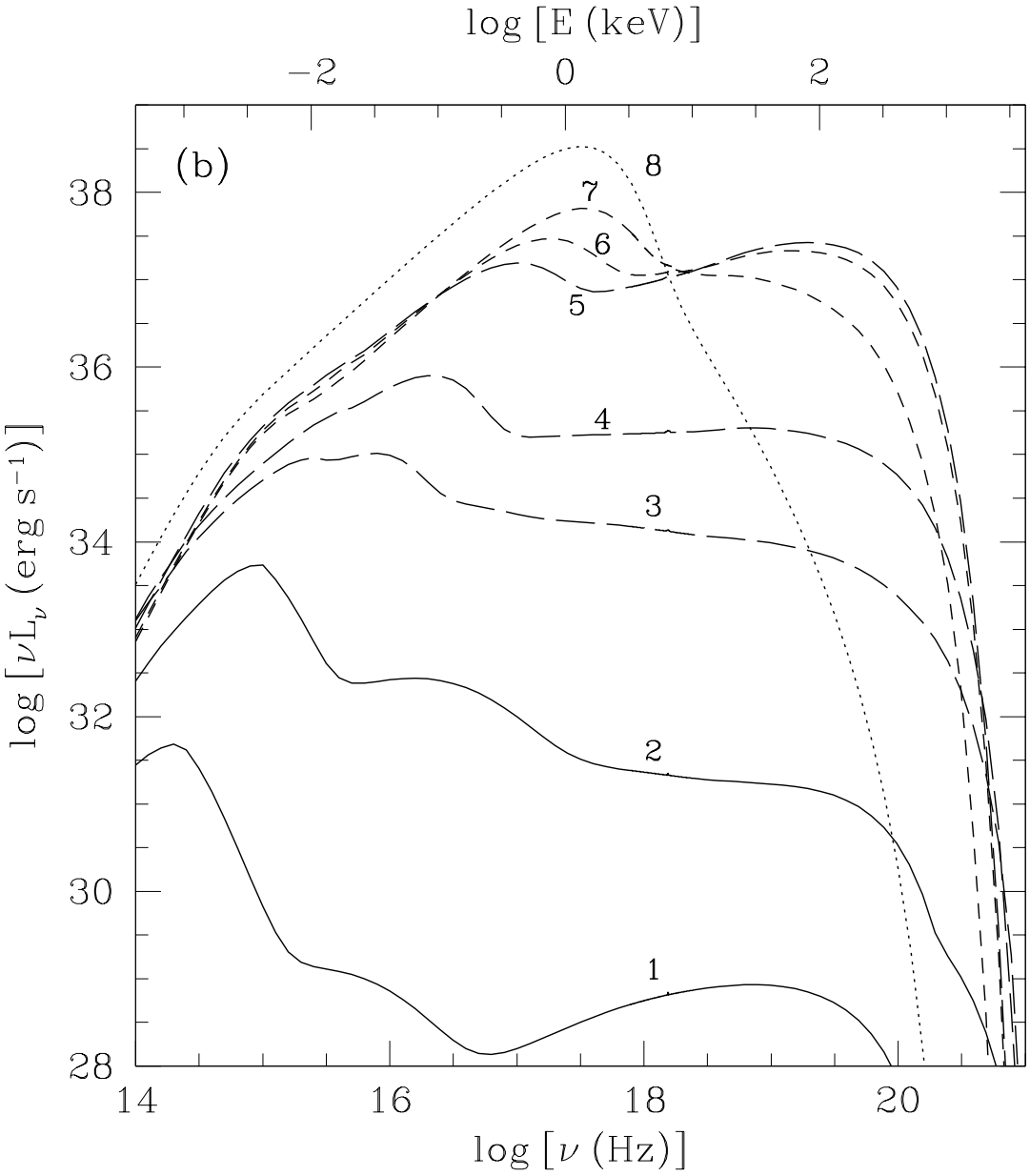

Fig. 1.— (b) 1–(3.9, 10^{-4}); 2–(3.2, 10^{-3}); 3–(2.3, 0.01); 4–(1.9, 0.03); 5–(1.5, 0.11); 6–(1.0, 0.12); 7–(0.5, 0.12); 8–(0.5, 0.4).

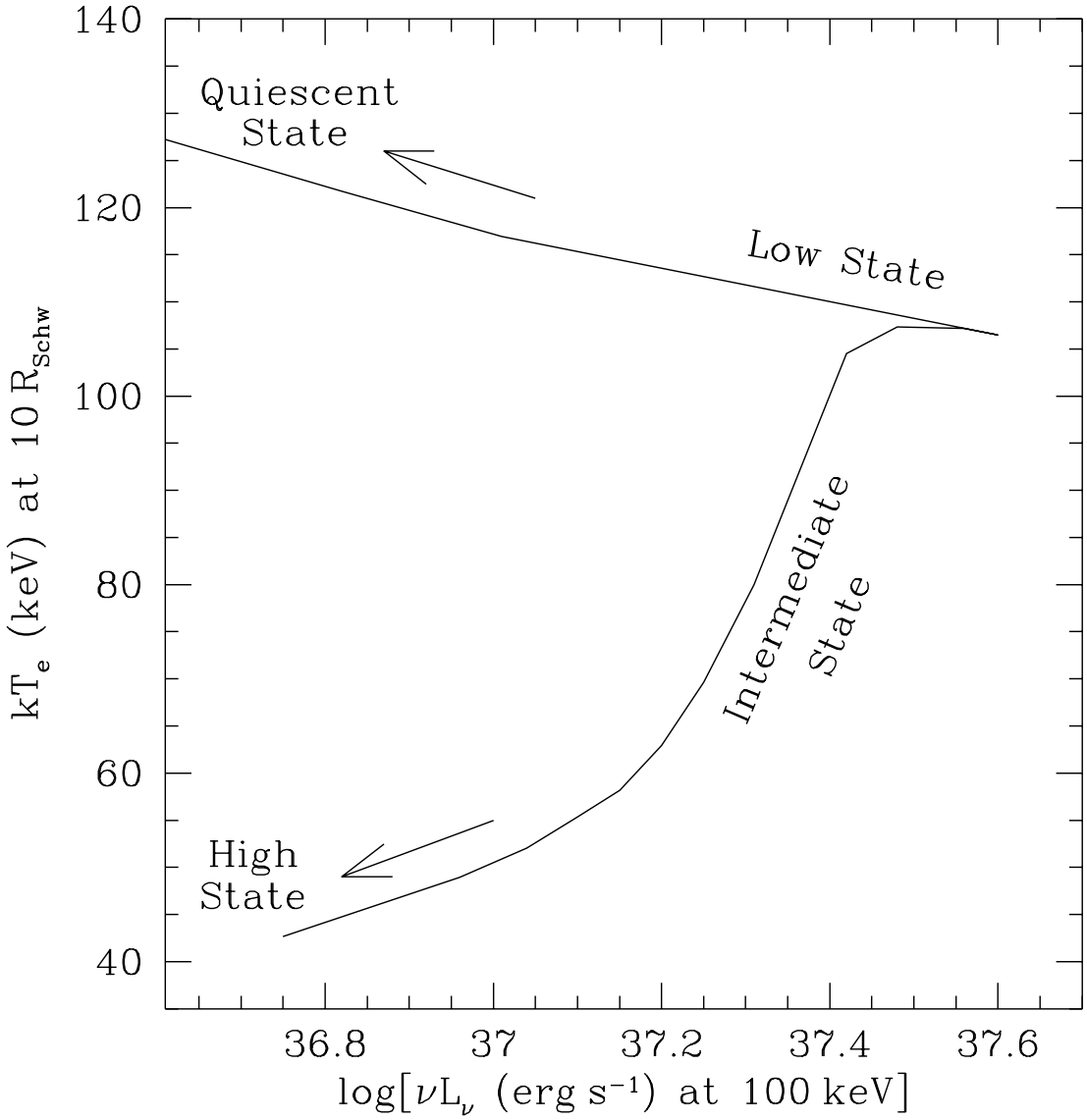

Fig. 2.— The electron temperature in an ADAF at $10R_{\rm Schw}$ plotted vs. the specific luminosity at 100 keV. Note that the two quantities are correlated in the intermediate and high spectral states and anticorrelated in the quiescent and low states.

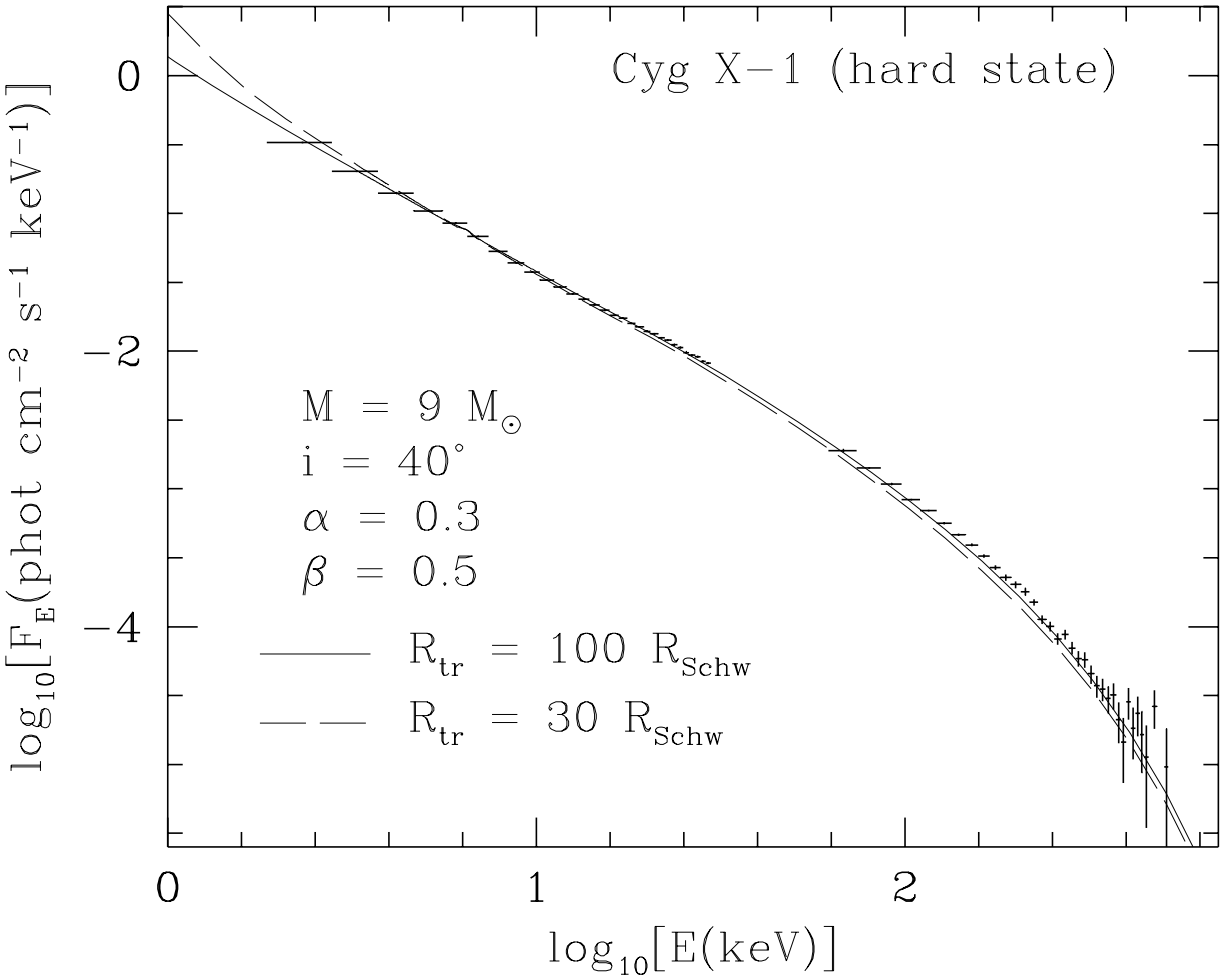

Fig. 3.— Low/hard state spectra of Cyg X-1 observed by Ginga and OSSE on July 6 1991 (from Gierliński et al. 1997) shown together with two model spectra corresponding to $r_{\rm tr} = 100$ (solid curve) and $r_{\rm tr} = 30$ (dashed curve). Both model spectra are normalized by a factor of 0.37.

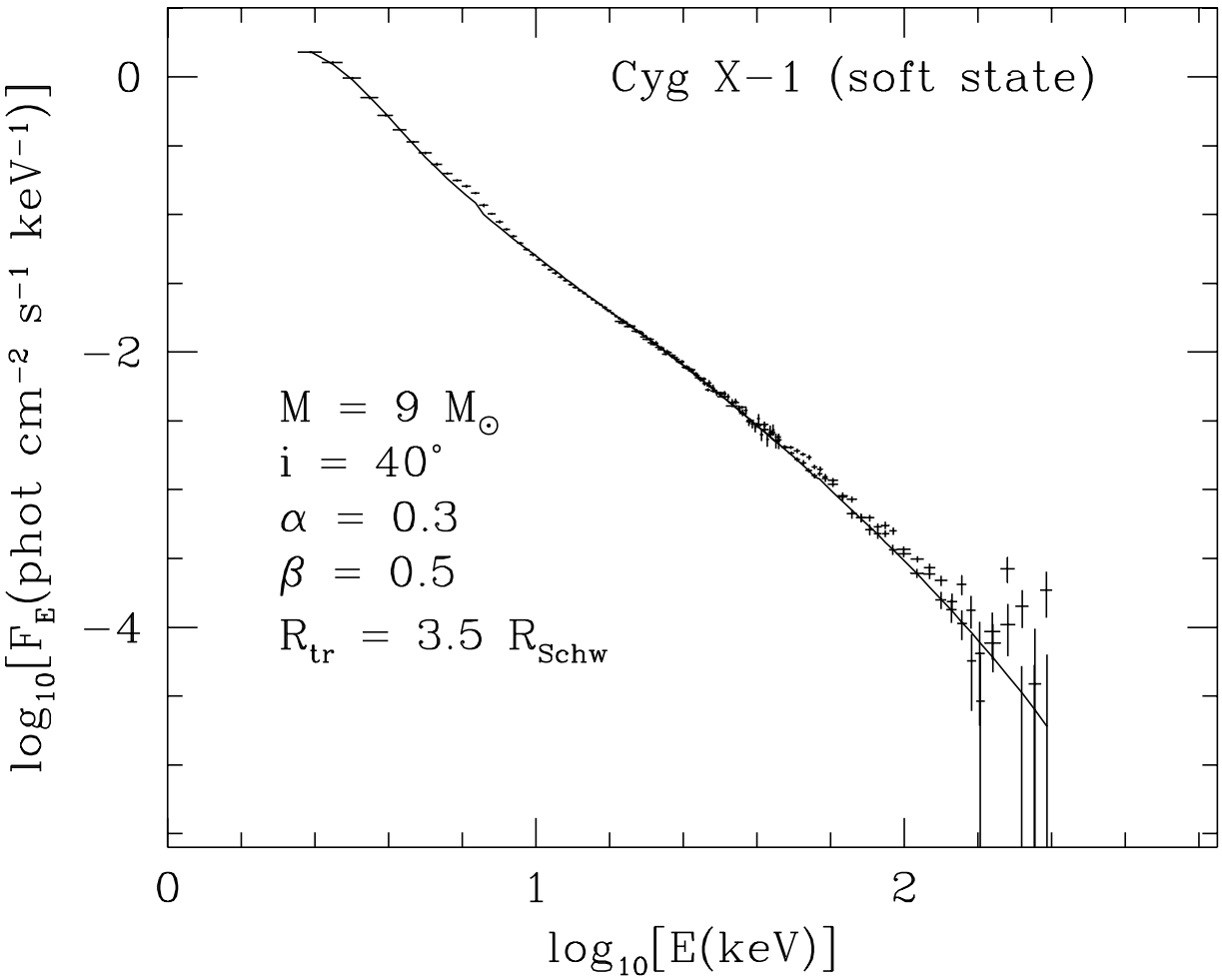

Fig. 4.— Combined PCA/HEXTE high/soft state spectrum of Cyg X-1 observed on 1996 May 22 plotted together with the best fitting model spectrum corresponding to the intermediate state, normalized by a factor of 0.48.

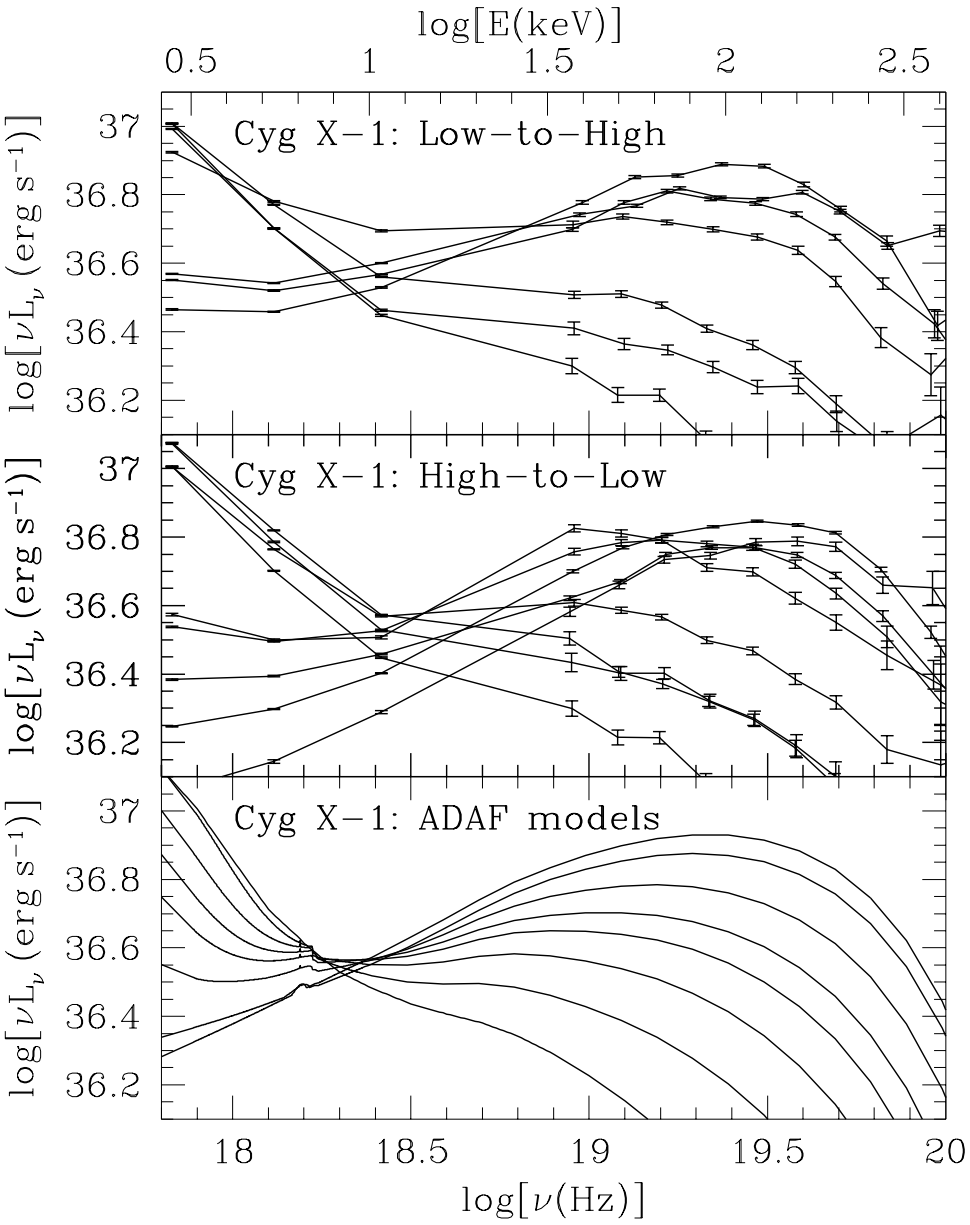

Fig. 5.— Broadband simultaneous RXTE/ASM (1.3-12 keV) and BATSE (20-600 keV) spectra of Cyg X-1 observed during its 1996 state transition shown together with the transition sequence predicted by the EMN model. (a) Spectra observed during the low–high state transition (TJD 10176-10272). Note that the lines connecting the data points are not fits to the data, but are meant simply to guide the eye. (b) Spectra observed during the high–low state transition (TJD 10273-10369). (c) Sequence of intermediate and high state spectra computed for a model with $m = 9$, $i = 40°$, $\alpha = 0.3$, $\beta = 0.5$ and the following values of $r_{\rm tr}$ (upper to lower spectra at 100 keV): 100, 30, 10, 6.3, 5, 4, 3.2, 3. All model spectra have been normalized by a factor of 0.33.

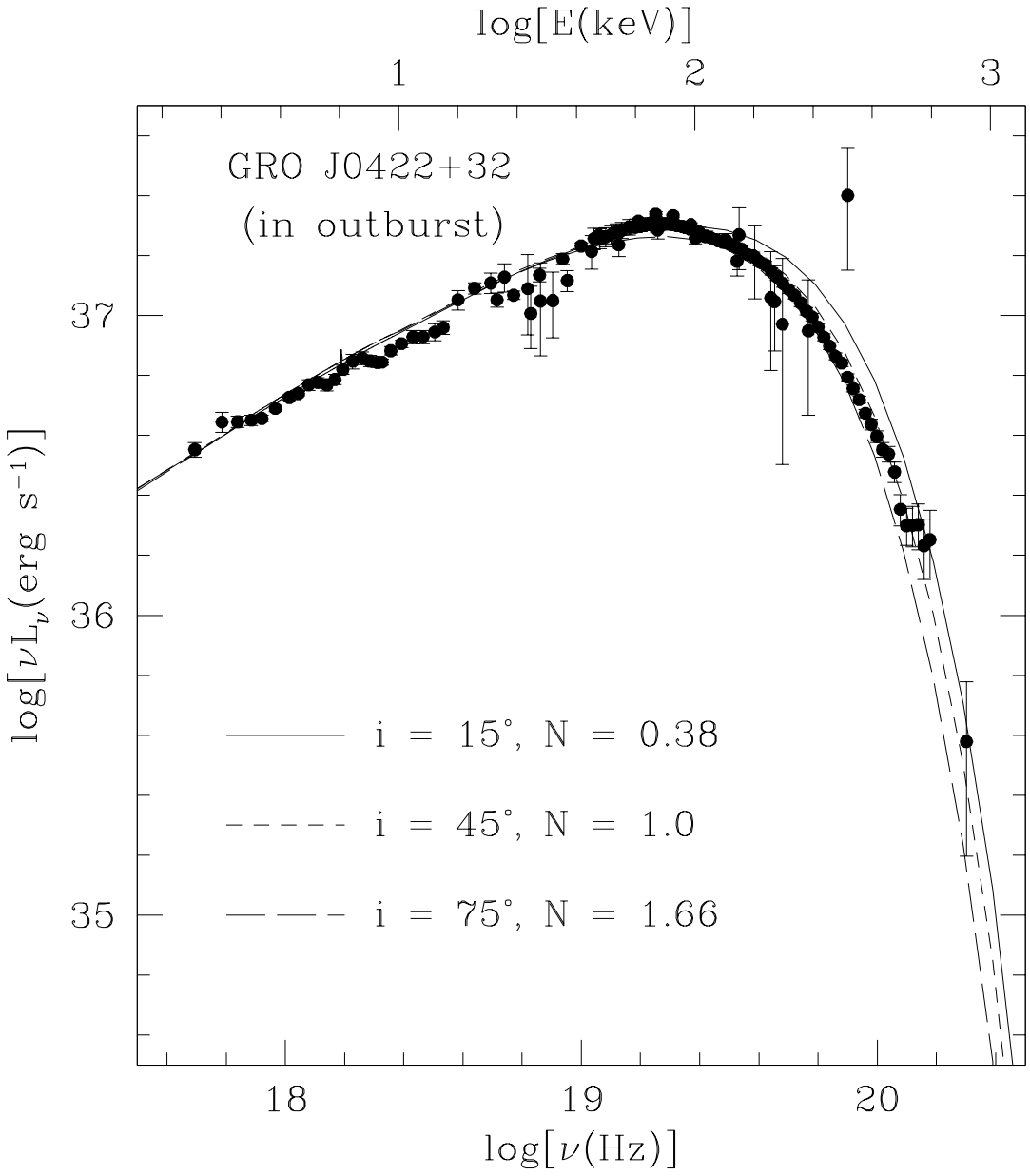

Fig. 6.— The combined TTM (2-20 keV), HEXE (20-200 keV) and OSSE (50-600 keV) spectrum of GRO J0422+32 observed between 1992 August 29 and September 2, plotted together with the model spectra computed for $m = 9$, $\alpha = 0.3$, $\beta = 0.5$, $r_{\rm tr} = 10^4$, $\dot{m} = 0.1$ and inclination i and normalization factor N as indicated on the figure. Though all three spectra fit the data reasonably well, the one computed with $i = 45^\circ$ reproduces both the overall luminosity of the source and the shape of the high energy cut-off.

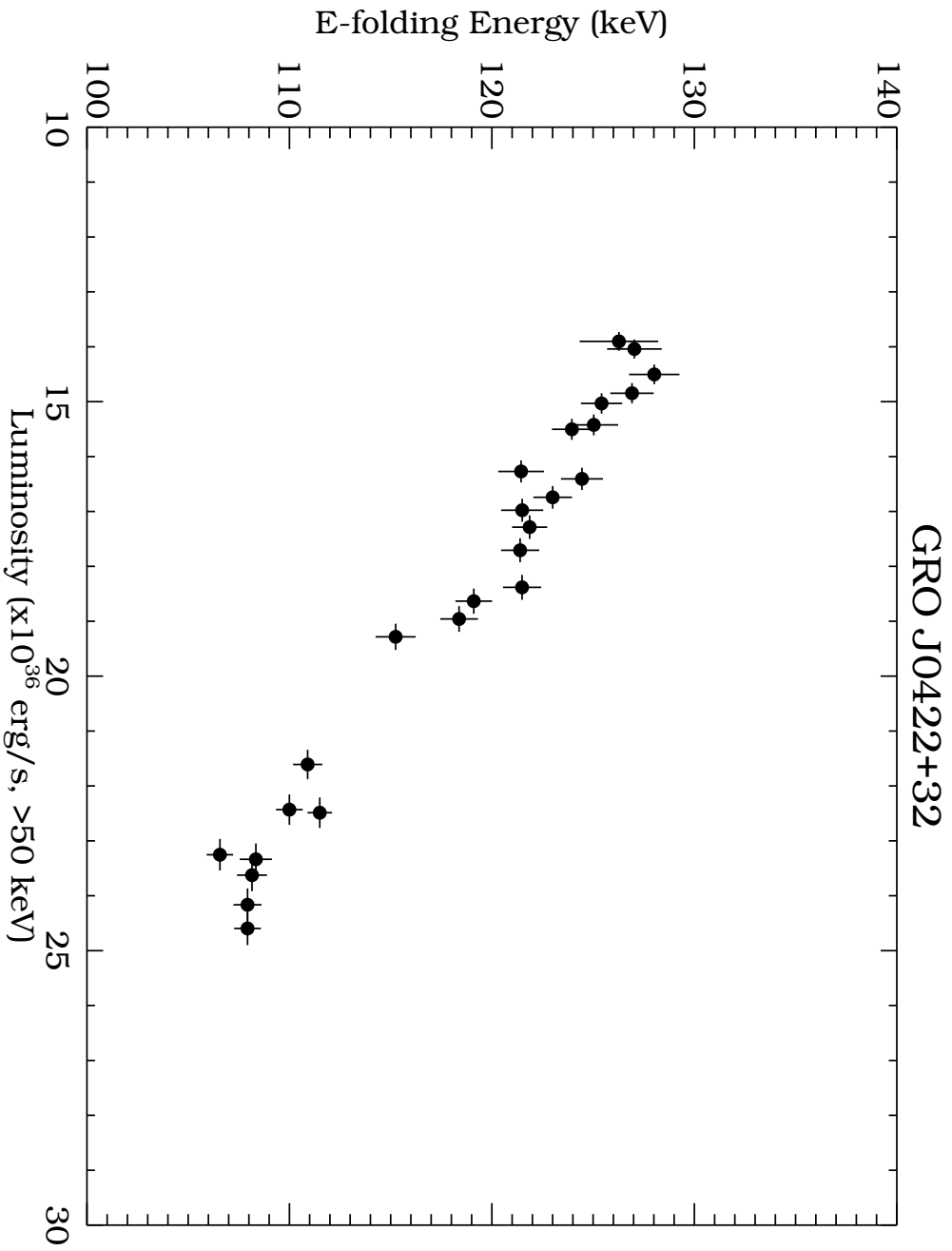

Fig. 7.— The e-folding energy derived from the OSSE spectra of GRO J0422+32 plotted against the γ-ray luminosity (60-1000 keV). The source was observed between 1992 August 11 and Sept 17, spanning the interval from the peak of the outburst to approximately half maximum intensity. During this time the γ-ray flux from GRO J0422+32 decreased monotonically. Note the clear anticorrelation between the e-folding energy and high energy flux, indicating that the source made a transition from the low state toward the quiescent state (see Figure 2).

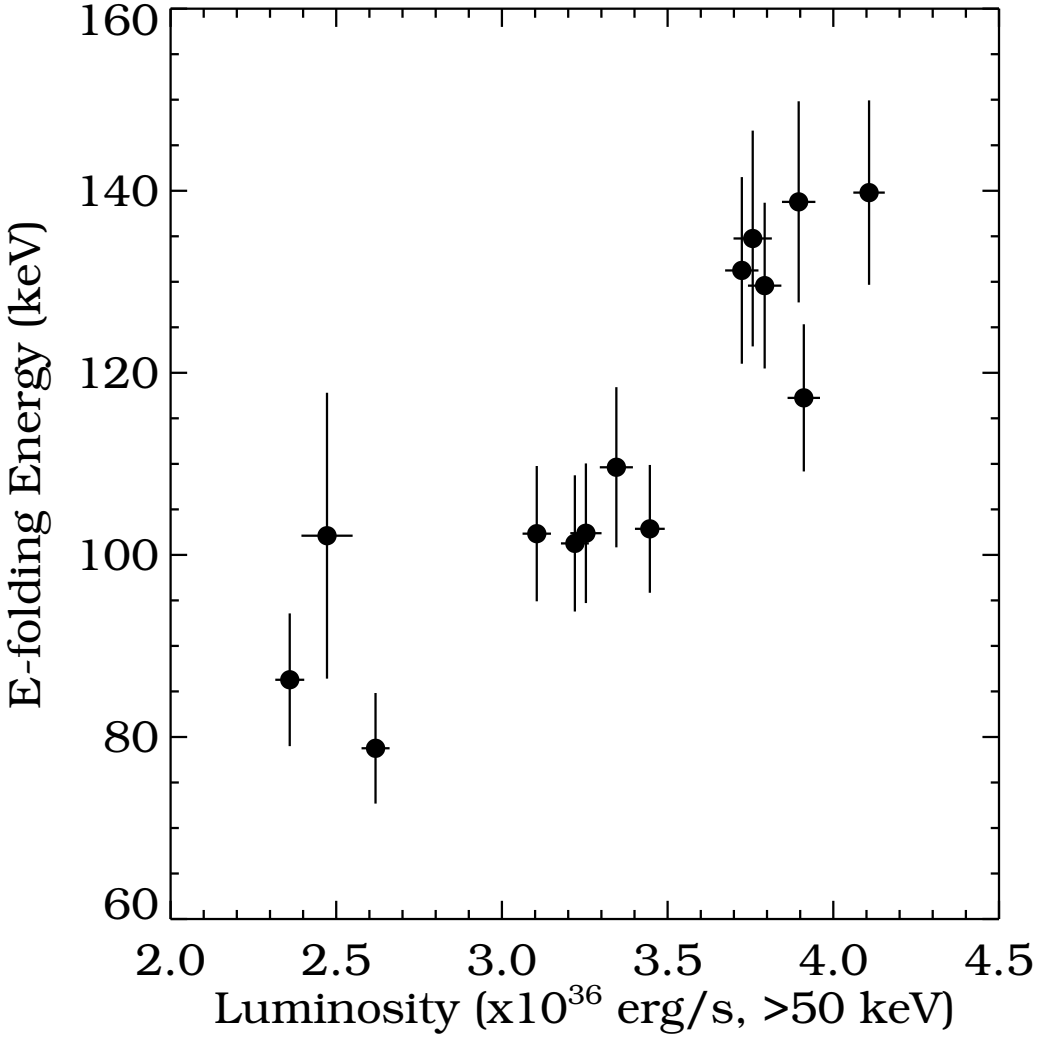

Fig. 8.— The e-folding energy derived from the OSSE spectra of GRO J1719−24 plotted against the γ-ray luminosity (60-1000 keV). The observations were made near the peak of the second smaller flare (1995 Feb 1-14), during the near monotonic decrease of the γ-ray flux. As opposed to GRO J0422+32, this source shows an almost linear correlation between the e-folding energy and high energy flux, indicating that the source made a transition from the intermediate state to the high state (see Figure 2).